

Chapter 2

Basic MR Physics: Considerations for Behavioral Medicine and Neuropsychology

Edward G. Walsh

Origin of the Nuclear Induction Signal

From its beginnings as a medical imaging modality in the mid-1980s, magnetic resonance imaging (MRI) has become a dominant modality, combining the ability to provide both structural and physiologic information. The physical principles relating to the production of the nuclear signal were described in the mid-twentieth century, with the publication of the first demonstration of nuclear induction taking place in 1946.¹⁻³

Nuclear induction is understood using a quantum mechanical approach. Fortunately, the magnetic resonance phenomenon also lends itself to a classical formalism when dealing with a large number of nuclei, which is always the case when discussing magnetic resonance as an imaging modality. Protons possess properties of mass and momentum, and a quantized property known as spin angular momentum. Spin is a property of both individual particles, and of nuclei. Not all nuclei possess spin. The basic conditions for the existence of spin:

- Nuclei with even mass and charge numbers have zero spin (e.g., ^{12}C).
- Nuclei with odd mass numbers have half integral spin (e.g., ^{13}C).
- Nuclei with odd mass and even charge numbers have integral spin (e.g., ^{14}N).

^{13}C and ^{31}P , for example, have been used for in vivo magnetic resonance spectroscopic studies. For MRI,

the ^1H nucleus is used due to its abundance and favorable molecular dynamics of water molecules. As a quantized property, nuclear spin can take on only specific values, related to the composition of the nucleus. In the case of ^1H , the nuclear spin is $1/2$, because the nucleus consists of a single proton, which is a spin $1/2$ particle. A consequence of the spin is the generation of a magnetic moment. The spin number of a nucleus dictates the number of orientations that the moment axis can take. For a spin $1/2$ particle, there are two possible orientations of the spin axis. In the absence of an external magnetic field, the energy states associated with the two orientations are identical (said to be degenerate). No difference in energy exists between the orientations. This degeneracy is lifted when a nucleus is placed in an external magnetic field.

Prior to placement of a sample (or patient) in a magnetic field (designated \mathbf{B}_0), the orientation of the spin axes is random, and the nuclear magnetic dipoles essentially sum to zero, so no net magnetization is developed. When the sample (or patient) is placed in the static field of an MRI scanner, the degeneracy is lifted and the hydrogen nuclei (protons) assume one of the two states describing the alignment of their magnetic moments: either aligned with or against the static field of the scanner (Fig. 2.1). Owing to the fact that the thermal energy of the system is larger than the energy difference between the two alignment states, the population of spins aligned against the static field is nearly identical to the population aligned with the field. Since alignment in the direction of \mathbf{B}_0 represents the lower energy state, there is a slight surplus (a few ppm) of spins aligned in the direction of \mathbf{B}_0 , and a net magnetization in the direction of \mathbf{B}_0 is developed within the sample. This is referred to as polarization. Establishment of this distribution

E.G. Walsh (✉)
Brown University, Departments of Neuroscience and Diagnostic Imaging, Institute for Brain Science, Providence, RI, USA
e-mail: Edward_Walsh@brown.edu

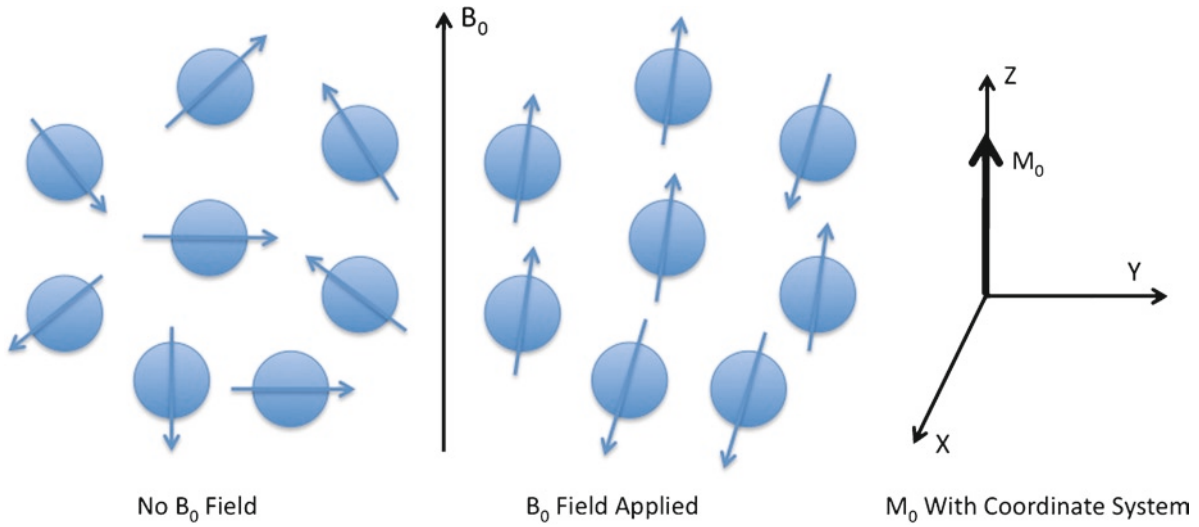


Fig. 2.1 *Left:* In the absence of an applied magnetic field, nuclear magnetic moments are randomly oriented and sum to zero. *Middle:* Application of magnetic field (\mathbf{B}_0) causes polarization

and resultant sample magnetization. *Right:* Coordinate system used to describe magnetic resonance experiments. Magnetization developed from polarization is defined as being in the z -direction

requires some time, and when the process is complete, the system is said to be in its equilibrium state. Static field strength is expressed in units of Tesla (T). 1 T=10,000 Gauss (G). By way of comparison, the Earth's magnetic field strength is about 0.5 G. Increasing the strength of \mathbf{B}_0 from 1.5 to 3 T, for example, increases the difference in the size of the two spin populations, and therefore the magnitude of the sample magnetization (designated \mathbf{M}_0). The maximum size of the MR signal is proportional to \mathbf{M}_0 , so increasing field strength (\mathbf{B}_0) increases \mathbf{M}_0 and therefore the maximum size of the MR signal. For clinical scanners, field strength ranges from 0.35 (for some open permanent magnet designs) to 3 T. Scanners used in research applications can have higher field strengths. As of this publication, the Food and Drug Administration (FDA) has defined field strengths greater than 8 T as representing a significant risk for humans over 1 month in age.

There is a second aspect to the behavior of the spins in an external magnetic field. The alignment of the spins with and against \mathbf{B}_0 is not complete, in that an angle exists between the nuclear magnetic moments and \mathbf{B}_0 . This results in a precession of the moment about \mathbf{B}_0 . The frequency of this precession is known as the Larmor frequency and is given by:

$$\omega_L = \gamma B_0 \quad (2.1)$$

where the constant of proportionality γ is known as the gyromagnetic ratio and is unique for each isotope. For ^1H , $\gamma=42.58 \text{ MHz/T}$, so at clinical field strengths, the range of precession frequencies falls within the range of frequencies used for radio communications. It is important to note that the splitting of the spin population into the two states, and resulting precession, does not result in a detectable MR signal. At this point, the phases of the individual spins in precession are random, so the component of the sample magnetization perpendicular to \mathbf{B}_0 is zero.

The MRI process involves the manipulation of the magnetization vector \mathbf{M} in order to produce a detectable signal. This process can be described using a classical formalism. To begin with, once a sample has been placed in the scanner, the net sample magnetization \mathbf{M}_0 is developed over a few seconds. \mathbf{M}_0 is aligned with \mathbf{B}_0 as shown in Fig. 2.1. In the Cartesian reference frame, \mathbf{B}_0 is defined as being in the z -direction. In conventional scanners, the z -direction is along the bore, with the x -direction being left-right and the y -direction being up-down. A rotating reference frame (x,y -axes rotate about the z -axis at the Larmor frequency) greatly simplifies the description of the imaging process and is normally

used in analyzing MRI acquisition sequences. A radiofrequency magnetic field (designated \mathbf{B}_1) applied perpendicular to \mathbf{B}_0 with a frequency equal to the Larmor frequency will cause some spins in the low-energy state to move to the high-energy state, at the same time placing the precession of the spins in phase. The result is that the vector \mathbf{M} is seen to rotate into the x - y plane in the rotating reference frame (Fig. 2.2). In a stationary reference frame \mathbf{M} would be seen to be precessing at the Larmor frequency as it tips down toward the x - y axis plane (typically referred to as the transverse plane since it is perpendicular to \mathbf{B}_0). This is described as being a *resonance* phenomenon since the application of a \mathbf{B}_1 field at a frequency away from the Larmor frequency will not have an effect on the spin population and therefore no action on \mathbf{M} .

A radiofrequency resonator, or coil, is configured and oriented to produce a \mathbf{B}_1 field perpendicular to \mathbf{B}_0 . This coil can also detect the precessing magnetization \mathbf{M} . The precessing \mathbf{M} will induce a voltage in the coil at the precession (Larmor) frequency that can be amplified and processed. The resonator itself is a resonant circuit at the Larmor frequency. This tuning provides for improved response (stronger signal) at the Larmor frequency and for attenuation of noise away from the Larmor frequency.

The angle (θ) through which \mathbf{M} rotates away from the z -axis while under the influence of \mathbf{B}_1 is known as the flip angle and is given by:

$$\theta = \gamma B_1 t \quad (2.2)$$

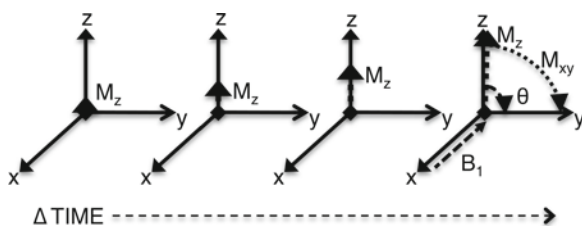


Fig. 2.2 Development of longitudinal magnetization over time following placement of a sample in a static magnetic field (\mathbf{B}_0). *Right:* Delivery of an RF pulse (\mathbf{B}_1) rotates magnetization into the transverse plane by an angle θ . If the x , y -axes rotate about the z -axis at the Larmor frequency, precession of the \mathbf{M} vector is removed simplifying visualization of relaxation and the effects of RF pulses. This also reflects the recovery of magnetization following a 90° pulse. Delivering another pulse during the recovery will produce a signal with intensity proportional to the degree of recovery

where B_1 is the strength of the radiofrequency field and t is its duration. Flip angle is an important adjustable contrast parameter for some imaging sequences as will be seen later. Note that like \mathbf{B}_0 , \mathbf{B}_1 is a vector quantity and has both magnitude and direction.

Relaxation

When the spin population has been perturbed by the application of a \mathbf{B}_1 field, this new distribution does not remain indefinitely following the termination of \mathbf{B}_1 . Instead, the equilibrium distribution will re-establish itself over time. The rate at which the equilibrium is restored is given by the longitudinal relaxation time constant, designated T_1 . In the rotating reference frame, termination of \mathbf{B}_1 stops the rotation of \mathbf{M} . In the absence of \mathbf{B}_1 , the \mathbf{M} vector will be seen to begin moving back toward its equilibrium position on the z -axis (aligned with \mathbf{B}_0). This recovery (often referred to as relaxation) is described by the longitudinal Bloch equation¹:

$$\frac{dM_z}{dt} = \frac{M_0 - M_z}{T_1} \quad (2.3)$$

where M_z is the longitudinal (z) component of the magnetization (\mathbf{M}), M_0 is the equilibrium magnetization (prior to any excitation), and T_1 is the longitudinal relaxation time constant, which is a material-dependent property. Since molecules tumble and translate, a given spin is subjected to a fluctuating magnetic field owing to the motion of nearby nuclear magnetic moments. If the frequency of fluctuation approaches the Larmor frequency, for example, relaxation becomes very efficient and T_1 will be very short. This is the effect exploited by contrast agents such as Gd-DTPA that act to reduce the T_1 of tissues in which they accumulate.

There is a second relaxation process at work simultaneously with the one just described. This process relates to the individual spin precession frequencies. Recall that ω_L varies with the external field strength. A given nucleus is also in the presence of other nuclei, and electrons, and is therefore subject to tiny fluctuations in the field that it experiences (due to the magnetic moments of nearby particles). These in turn produce tiny fluctuations in ω_L . Since

these interactions are essentially random, the effect is that the spins gradually go out of phase, and therefore the transverse summation of the magnetic moments decays over time, resulting in a reduction in the transverse component of \mathbf{M} (commonly known as \mathbf{M}_{xy}). This is seen as a loss in the amplitude of the observed signal coming from the resonator. Such signals are referred to as free induction decays (FID). The decay rate constant for this process is known as T_2 , the spin–spin relaxation rate constant. The transverse magnetization decay is given by the transverse Bloch equation¹:

$$\frac{dM_{xy}}{dt} = \frac{-M_{xy}}{T_2} \quad (2.4)$$

The preceding describes the process based on the true T_2 of the sample, the decay rate characteristic to the material. There is another process to consider, and it relates to the fact that the static field produced by the scanner magnet is not perfectly uniform (homogeneous). The actual strength of \mathbf{B}_0 can vary by a few ppm over the imaging volume. This field imperfection produces a corresponding distribution in ω_L across the sample, and this distribution also contributes to signal dephasing. Field variations also result from the presence of materials with differing magnetic susceptibility (differing tendency to generate magnetization). The observed decay rate of the signal in the presence of field inhomogeneity is given by the rate constant T_2^* . These two transverse relaxation rates are related as:

$$\frac{1}{T_2^*} = \frac{1}{T_2} + \frac{1}{T_2'} \quad (2.5)$$

where T_2' is the contribution resulting from field imperfections. It will be seen that T_2^* relaxation processes play a major role in functional MRI of the brain. The decay of the transverse signal is given by the same expression (2.4) used for transverse decay, substituting T_2^* for T_2 . It will be shown later that it is possible to separate T_2 and T_2^* using appropriate pulse sequences. Scanners also provide a mechanism for improving the uniformity of the field. The process typically referred to as shimming involves the use of field gradient coils to modify \mathbf{B}_0 in order to maximize homogeneity over the volume to be scanned.

Values for T_1 and T_2 depend on field strength and material properties (e.g., molecular correlation times).

Of benefit for MR imaging is that different tissues often have different relaxation time constants. These differences can be exploited for the purpose of generating soft tissue contrast. For example, at 3 T the T_1 of grey matter is about 1,400 ms, while for white matter T_1 is about 800 ms. This difference allows for the generation of excellent contrast between grey and white matter without the use of any exogenous contrast agent.

Now it is appropriate to introduce the concept of flip angle (θ) in the context of signal strength and relaxation. Of particular interest in structural brain imaging is the generation of contrast among grey matter, white matter, and cerebrospinal fluid (CSF). Turning first to longitudinal magnetization, there are two flip angle examples that are relevant for generating contrast. Recall that flip angle is the extent to which the sample magnetization vector \mathbf{M} is rotated by an RF excitation (\mathbf{B}_1). If \mathbf{M} is rotated onto the transverse (x – y) plane, a 90° excitation (pulse) has been delivered. In this case, the longitudinal magnetization M_z is zero, and the system is said to be saturated (the populations of spins in the high- and low-energy states are equal). It is possible to continue rotating \mathbf{M} past this point, continuing the excitation until \mathbf{M} lies on the negative z -axis. In this case, a 180° excitation (pulse) has been delivered, and the system is said to be inverted. The inversion excitation is so named since the populations of spins in the two energy states have been exchanged (inverted), with the (same equilibrium) majority of spins now aligned against the field. Based on these excitations, the longitudinal magnetization as a function of time is given as:

$$M_z(t) = M_0(1 - e^{-t/T_1}), \quad \theta = 90^\circ \quad (2.6)$$

$$M_z(t) = M_0(1 - 2e^{-t/T_1}), \quad \theta = 180^\circ \quad (2.7)$$

where t is the elapsed time following the termination of the RF excitation. For the transverse magnetization following a 90° pulse:

$$M_{xy}(t) = M_0 e^{-t/T_2^*} \quad (2.8)$$

where t again represents the elapsed time following the termination of the RF excitation. These expressions (which are solutions to the Bloch equations) assume that the RF pulse is delivered with the spin system at equilibrium (full longitudinal recovery). In imaging studies, it is generally not practical to deliver all excita-

tions with the spin system at equilibrium, as the scans would become prohibitively long.

We now have the information available to measure the T_1 of a sample. Returning to Fig. 2.2, a 90° or 180° can be delivered, followed by a gradient pulse to destroy (spoil) any transverse signal. Gradients will be discussed later, but suffice it to say at this point that turning on a field gradient produces a huge field inhomogeneity that results in very rapid signal dephasing (loss of the transverse component of \mathbf{M}). Following this, a delay (t) is allowed, during which some longitudinal relaxation takes place. If another 90° pulse is delivered (readout pulse), and the signal received, it is

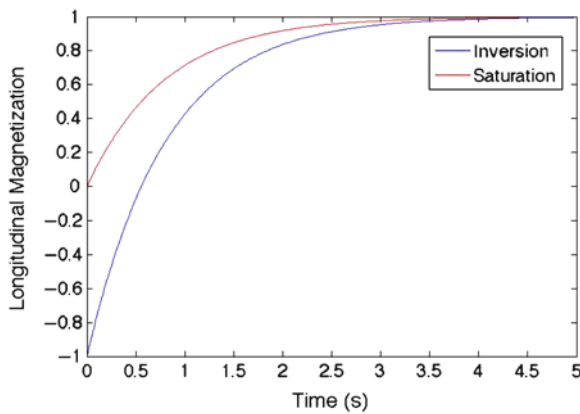


Fig. 2.3 Magnetization vs. postsaturation or inversion time of a material with a T_1 of 1 s. Use of inversion doubles the dynamic range in the longitudinal magnetization

seen that the transverse magnetization intensity is proportional to that of the longitudinal magnetization at the time of the delivery of the readout pulse. If signals are obtained for a range of values of t , the T_1 of the sample (or tissue) can be determined by a curve fit (signal intensity vs. t) to (2.6) (Fig. 2.3). This is T_1 measurement by saturation recovery. It is also possible to use a 180° (inversion) pulse prior to the readout pulse, in which case (2.7) is used. This inversion recovery method has the advantage of doubling the dynamic range of longitudinal magnetization and produces more accurate T_1 estimation (or more contrast in images). It will be seen that these methods can also produce soft tissue contrast, for example, between grey and white matter since they possess different T_1 values. For imaging, the initial 90° or 180° pulse is known as a contrast pulse, or contrast preparation pulse, and will be followed by a pulse sequence (readout sequence) for reading spatially encoded image information.

Turning now to T_2 and T_2^* , it was noted that the first value is a property of the material under consideration, and the second adds the effects of static field inhomogeneity. To separate these two effects, a pulse sequence is needed that can “undo” the effect of the static (time invariant) inhomogeneities. Such a sequence can be formed using two RF pulses, a 90° pulse followed by a 180° degree pulse. This is shown in Fig. 2.4. Note that there are no spoiler gradients. The transverse magnetization is preserved throughout the sequence. As shown

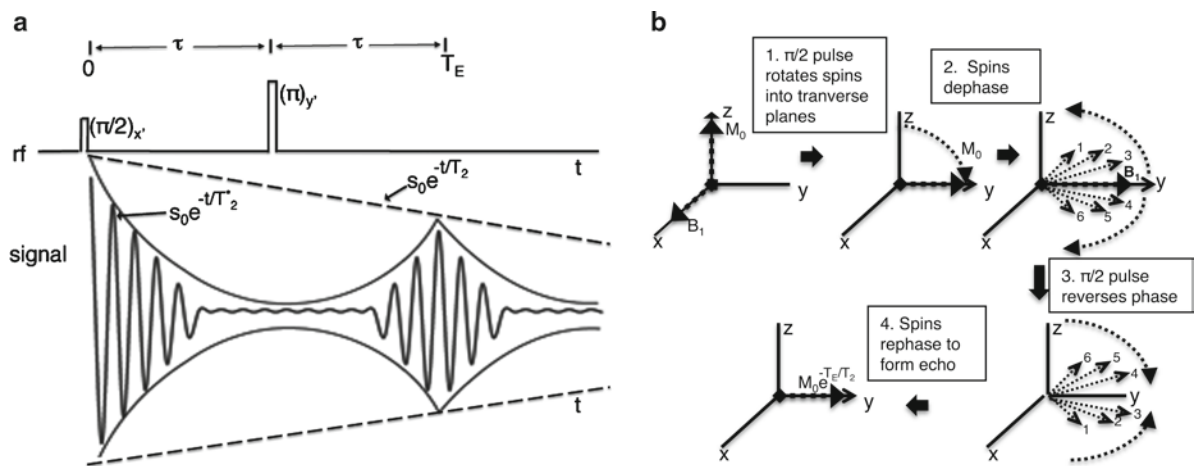


Fig. 2.4 Left: Spin echo pulse and signal diagram. The 90° ($\pi/2$) pulse produces a free induction decay (FID) that decays according to T_2^* . The 180° (π) pulse refocuses an echo at the echo time with

amplitude reflecting the true T_2 . Right: Effect of the refocusing pulse on the temporal evolution of magnetization in different parts of an inhomogeneous field

prescription of image planes based on a fast scout scan. The operator simply moves an outline overlay over the displayed scout images to define the tomographic slices to be obtained in the subsequent scan. The scanner software takes care of the mathematics relating the selected image planes to the standard orthogonal views.

In the previous discussions, the processes of signal formation and decay were discussed. These signals did not contain any spatial information, and arose from the entire sample (or patient) in the scanner. In order to produce tomographic images, it is necessary to have three dimensions of spatial encoding imposed on the MR signals. This is accomplished using linear field gradients,⁵⁻⁸ which can be switched on and off very rapidly. Every patient scanner is equipped with a set of field windings that can generate a linear field gradient on each (x, y, z) axis. The individual gradient channels (one for each direction) can be independently switched. These gradient systems are manufactured to high tolerances such that a field linearity specification of at least 95% can be achieved, typically over a diameter spherical volume (DSV) of 45–50 cm. The purpose of the field gradients is to cause the static field (\mathbf{B}_0) to vary in a linear fashion with distance on each axis from the central point of the scanner's defined imaging volume. The consequence of turning on a gradient is that the Larmor frequency (ω_0) will also vary in a linear fashion with position along the gradient direction. The gradient systems are designed such that there is a point where the field does not vary when a gradient is turned on. This point is common for all three gradient axes, and is known as the isocenter. The isocenter represents the center of the DSV mentioned above. Figure 2.6 shows what happens when a gradient is turned on. On one side of isocenter, the field decreases,

and on the other, it increases, and at isocenter, it does not change. The \mathbf{B}_0 field strength and Larmor frequency now become:

$$B(x) = B_0 + Gx \quad (2.11)$$

$$\omega(x) = \gamma(B_0 + Gx) \quad (2.12)$$

where x is the distance from isocenter (and can be positive or negative depending on direction), and G is the gradient strength, typically expressed in units of G/cm or mT/m. Current clinical scanners can generate maximum field strengths ranging up to 4.5 G/cm (implications for rapid imaging performance). As opposed to the main field windings of superconducting magnets, the resistive gradient field windings are designed to be switched on and off very rapidly. Switching times are typically on the order of a few hundred microseconds. Gradient switching rate is also an important specification with respect to rapid imaging performance.

At this point it is necessary to introduce the Fourier transform. The Fourier transform is an operation that relates a time domain signal (the FID or spin echo) to its frequency spectrum. As noted above, delivering a 90° excitation to a water sample produces a monoexponential decay at the Larmor frequency. The Fourier transform of that signal will be a single peak at the Larmor frequency. If this simple spectrum is shifted to the rotating reference frame, the peak moves to a frequency of zero relative to the Larmor frequency.

It was previously mentioned that a gradient is a form of \mathbf{B}_0 inhomogeneity that results in very rapid decay of signals. For the time being, dephasing will be ignored in this discussion of spatial encoding. Dephasing, and the means of undoing it, will be discussed in the section on image acquisition pulse sequences. Delivering a 90° excitation produces a signal (FID) at the Larmor frequency that decays over time in a monoexponential fashion. Now consider the case of an object in the scanner, at some distance from isocenter in the x -direction (horizontal displacement). This object is a cube filled with water and is 1 cm on each side, and the center of the cube is 2 cm from the isocenter. After delivering the 90° excitation, a gradient in the x -direction is turned on with strength equal to 1 G/cm. The first observation is that the signal has a complex appearance (Fig. 2.7). Recall that the Larmor frequency now varies as a function of position in the x -direction. Since the object is of finite extent, it is producing a signal whose frequency

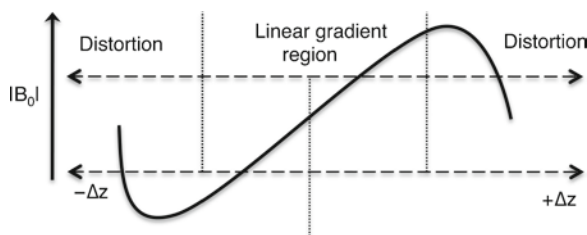


Fig. 2.6 Effect of linear gradient application. \mathbf{B}_0 and therefore the Larmor frequency vary linearly with distance from the isocenter (the point where \mathbf{B}_0 does not change when the gradient is switched on). Beyond the designed linear region of the field gradient coils, linearity is lost and geometric distortion results

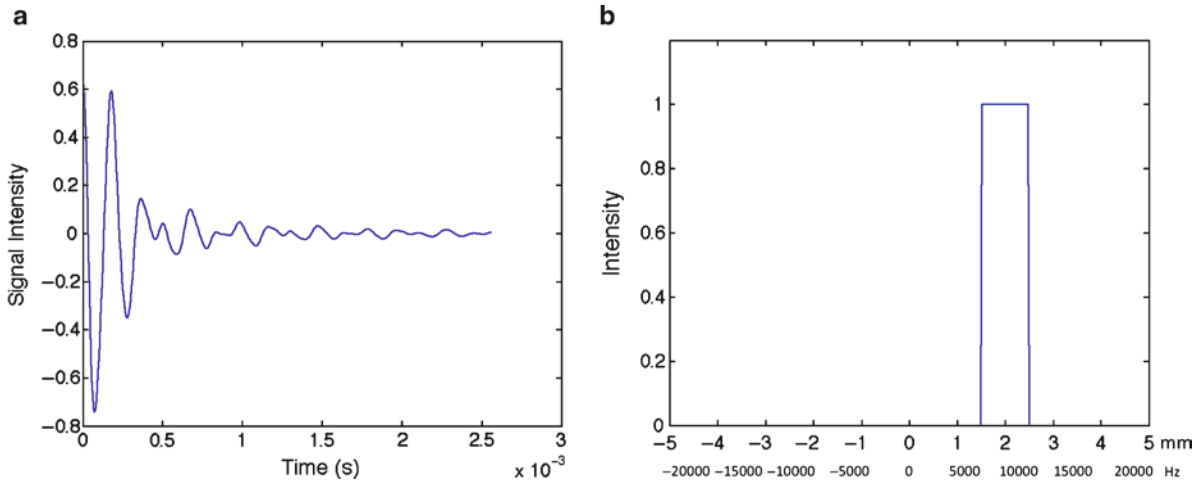


Fig. 2.7 *Top:* Signal produced by a 1 cm cube centered 2 cm from the isocenter. *Bottom:* Fourier transform of the signal showing frequency offset and extent

content is determined by its spatial distribution. The 1 cm cube is centered 2 cm from isocenter in the x -direction, therefore its spatial extent covers from 1.5 to 2.5 cm away from the isocenter. Using (2.12), this means that its extent in frequency space is 6,387–10,645 Hz. The Fourier transform shows the presence of signal covering that frequency range (Fig. 2.7). Signal intensity in the transform is uniform across that frequency range indicating that there is the same amount of material at all frequency components. There is no signal at any other frequency component since there was only a single object present. Thus, by turning on the gradient during signal collection, it was possible to determine the location and spatial extent of the object in the gradient direction by examining the frequency content of the signal (as well as estimating the shape of the object). This method is known as frequency encoding, and is used to spatially encode one of the in-plane dimensions of MR images.

MR imaging is a tomographic method, and in order to form tomographic images, it is necessary to possess the capability of exciting a thin slab of spins in the patient, while leaving everything else unaffected. We only want signal to arise from the slice of interest. How is this accomplished? Two components are needed: a gradient and a frequency selective RF excitation. Recall from the section “Origin of the Nuclear Induction Signal” that an RF excitation was delivered at the Larmor frequency to the entire sample to produce a FID. Now, a frequency selective pulse and a gradient will be used to limit the excitation to a defined

range of frequencies, corresponding to a specific spatial extent within the scanned object. With respect to the cube example, suppose we want to excite a slab of that cube, 5 mm wide, and centered within the cube. This would place the center of the excited slab 2 cm from isocenter in the x -direction. If we turn on the 1 G/cm gradient, a distance of 2 cm corresponds to a frequency offset of 8,516 Hz. We have also specified a slab thickness of 5 mm. A spatial extent of 5 mm centered at $x=2$ cm implies a frequency range of 7,452–9,581 Hz according to (2.12). This frequency range is contained completely within the frequency range for the entire cube. If we offset the frequency of the pulse by +8,516 Hz, its frequency will now correspond to the Larmor frequency at the center of the cube when the gradient is turned on. We need, however, to excite material over the range of frequencies just mentioned while excluding the rest. Therefore, we need an excitation that has a matching frequency content. Ideally, this excitation should have a frequency content of uniform intensity, beginning at +7,452 Hz and ending at +9,581 Hz, and having no other frequency components. This corresponds to a spectral width of 2,129 Hz. Taking the Fourier transform of such a rectangular function in frequency space results in a function in the time domain of the form:

$$B_1(t) = \frac{\sin(t)}{t} \quad (2.13)$$

This waveform is shown in Fig. 2.8, and it often referred to as a sinc pulse. The frequency content of

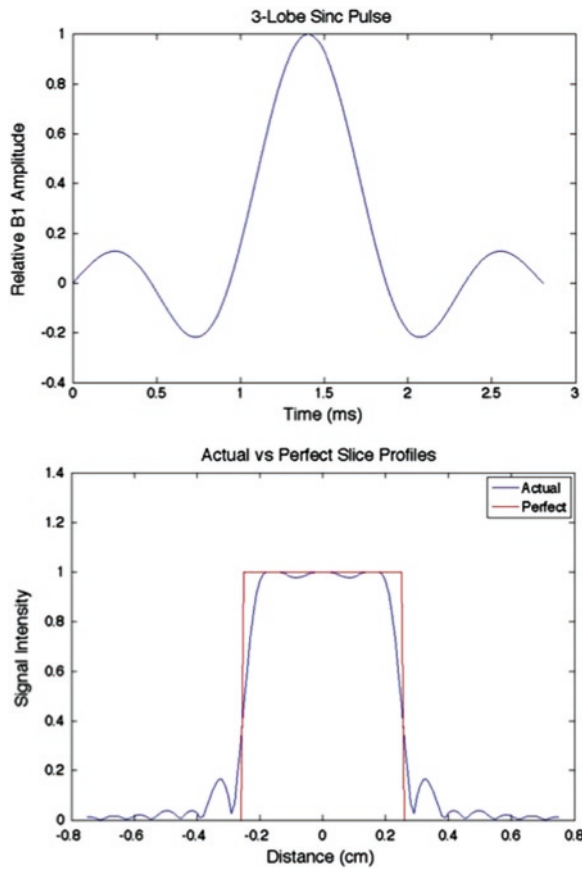


Fig. 2.8 *Top*: Typical three-cycle sinc pulse suitable for use in imaging sequences. *Bottom*: Corresponding slice profile showing the effects of truncation to limit pulse duration to an acceptable value

this pulse is determined by the interval between the zero-crossings of the waveform, with the bandwidth given by:

$$\Delta t = \frac{2}{\Delta f} \quad (2.14)$$

where Δt is the interval between zero-crossings and Δf is the bandwidth of the excitation. For the situation that we are currently considering, a bandwidth of 2,129 Hz is needed, and this corresponds to a zero-crossing interval of 0.939 ms. It should be noted at this point that the Fourier transform of a perfectly rectangular frequency function is a sinc function of infinite extent. RF excitations of infinite extent are not compatible with minimizing the duration of imaging studies for patient tolerance. Therefore, the sinc

pulse is truncated. A three-lobed waveform can be used as shown in Fig. 2.8. The duration of this pulse will be $3\Delta t$ or 2.82 ms. This pulse duration is compatible with MR imaging requirements. The consequence of truncating the sinc waveform is some degree of compromise in the excitation profile as shown in Fig. 2.8, where it is seen that there is some out-of-slice excitation accompanied by some “ripple” across the excited slab. This plot was generated using a numerical solution of the Bloch equation describing the motion of \mathbf{M} during the application of \mathbf{B}_1 (the RF excitation). For typical diagnostic imaging applications, these compromises have negligible effect on the images. Other waveforms are available for use when tailoring some aspect of the slice profile (e.g., out-of-slice excitation) to reduce interaction between neighboring slices.

From the foregoing, the procedure for slice positioning is clear. The plane of the slice is determined by the gradient that is turned on during delivery of the RF excitation: z -gradient gives a transverse slice, x -gradient gives a sagittal slice, and y -gradient gives a coronal slice. Gradient channels can be combined to give angulated slices. For example, if both the z - and y -gradients are turned on at the same time, and with the same strength during excitation, the resulting slice will be angulated 45° off the transverse orientation toward the coronal plane. Fortunately, the scanner operator does not have to perform any computations to obtain such angulations. Scanner software takes care of all calculations relating to gradient assignment in a user-transparent fashion. The operator simply selects the desired plane (and other relevant imaging parameters) and initiates the scan. Slice offset (from isocenter) and slice thickness are determined by the frequency offset and bandwidth of the RF excitation, and by the gradient strength. The dependencies are:

- For fixed gradient strength:
 - Increasing frequency offset increases slice offset
 - Increasing excitation bandwidth increases slice thickness
- For fixed frequency offset:
 - Increasing gradient strength reduces slice offset
 - Changing gradient polarity moves slice to opposite side of isocenter with the same offset distance

- For fixed excitation bandwidth:
 - Increasing gradient strength reduces slice thickness

The opposites apply for the above, so for example, decreasing gradient strength for fixed frequency offset increases the slice offset. As with gradient assignments for selection of image planes, these parameters are all set in a user-transparent fashion.

We now have two dimensions of spatial encoding and it remains to describe the process for generating the remaining in-plane spatial encoding, but first it will be helpful to introduce the concept of k -space.⁹ As seen in the discussion on frequency encoding, the profile of the object was revealed by taking the Fourier transform of the MR signal. For images, the Fourier transform relates the spatial representation of an object to its spatial frequency representation. In MR imaging, the signals that are being produced by the pulse sequences are pieces of the spatial frequency representation of the object. When the signals are assembled into a matrix, this matrix will be the frequency space representation of the viewable image. The Fourier transform is then applied to produce the viewable image

The remaining spatial encoding process is known as phase encoding, and is a bit more complicated in its

description than the processes for the other two dimensions in that it “builds up” information using a succession of gradient pulses. As shown in Fig. 2.9, the application of the short duration pulse changes the start location in the other in-plane direction for the k -line to be sampled. This phase shift is proportional to the shape, strength, and duration of the gradient pulse, and also on the distance of the object from the isocenter:

$$\Delta\phi = \gamma x \int_0^T G(t) dt \quad (2.15)$$

where $\Delta\phi$ is the phase shift, x is the distance from the isocenter, $G(t)$ is the gradient waveform shape function, and T is the duration of the gradient waveform. As seen in Fig. 2.9, if this process is repeated for a number of times, then it is possible to build up the same sort of information that was obtained using the frequency encode gradient applied in the other direction. The reason for using such a method to build information for one of the spatial dimensions will become clear in the discussion on image acquisition pulse sequences. With slice selection, frequency encoding, and phase encoding, we now have three orthogonal dimensions of spatial encoding that permit magnetic resonance to be used as a tomographic imaging modality. Two of the gradient assignments will always be used for in-plane spatial encoding and the third will be used for slice selection.

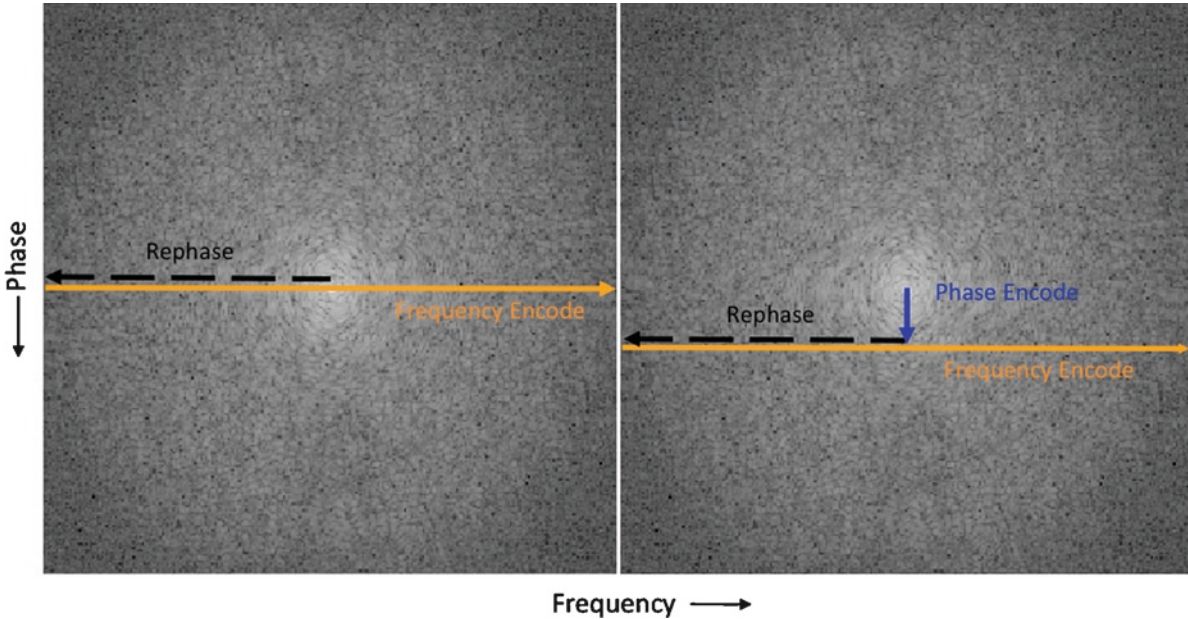


Fig. 2.9 Assembly of raw frequency space image data from MR signals acquired using multiple phase encode steps. The phase encode gradient pulse determines the starting position for the line to be read out using the frequency encoding gradient pulse

For the basic orthogonal planes (transverse, sagittal, and coronal), example gradient assignments would be:

- Axial (transverse)
 - Slice select = z
 - Frequency encode = y
 - Phase encode = x
- Sagittal
 - Slice select = x
 - Frequency encode = z
 - Phase encode = y
- Coronal
 - Slice select = y
 - Frequency encode = z
 - Phase encode = x

Note that for the two in-plane dimensions, the gradient assignments can be exchanged. In some applications, however, the patient geometry with respect to the desired field of view (FOV) dictates a specific assignment. The reason for this is that in the phase encode direction, any material outside of the specified FOV will be aliased back into the image (known as a fold-over artifact), a consequence of the Nyquist sampling condition.

Field of view in the frequency encode direction is determined by the range of frequencies that the scanner is instructed to receive. Recall from the preceding discussion that in the presence of a gradient, a range of Larmor frequency exists across an object. By restricting the range of frequencies that the scanner processes, the FOV can be limited. Specifically:

$$\text{FOV}_{\text{Freq}} = \frac{\text{SW}}{G_{\text{Freq}}} \quad (2.16)$$

where the FOV_{Freq} is in units of cm, SW is the spectral width (receive bandwidth) in units of Hz, and G_{Freq} is the frequency encode gradient strength in units of Hz/cm (for example, a 1 G/cm gradient corresponds to 4,258 Hz/cm). In the phase encode direction, the FOV is determined by the amount by which the area under the gradient waveform is incremented, which is also equal to the smallest gradient pulse to be applied:

$$\text{FOV}_{\text{Phase}} = \frac{1}{\gamma \int_0^T G_{\text{min}}(t) dt} \quad (2.17)$$

This increment insures that the Nyquist sampling theorem is observed in order to prevent aliasing. As with other parameters mentioned, the operator simply specifies the FOV, and the calculations for establishing encoding gradient strengths, durations, and the phase encode increment are performed in the background.

Although one cannot make a diagnosis from the frequency space representation of a brain image, there are certain characteristics to the k -space formalism that are helpful to know when selecting or designing acquisition sequences. Figure 2.10 shows how information is distributed in k -space. From the brain image example, it is seen that most of the signal energy is contained near the center of the k -space representation. The center of k -space ($k=0$) is the zero spatial frequency point. Spatial frequency, expressed in units of inverse distance (e.g., cm^{-1}) increases with increasing distance from $k=0$. Low spatial frequency information (near the center) deals primarily with contrast and representation of large areas. High spatial frequency information (away from $k=0$) deals with edges and fine details. How far out into k -space one samples determines the spatial resolution of the images. Figure 2.11 shows the effect of altering information content in k -space. In the low-pass filter example, it is seen that by removing high spatial frequency information, that contrast is preserved, but the image is blurred (edges and fine detail are lost) and has a lower effective spatial resolution. In the opposite case, removing the low spatial frequency information removes most of the contrast, but edge and fine detail information are preserved. The image acquisition pulse sequences are designed to fill k -space to a degree adequate for various applications within the limits of scanner performance and scan time tolerance.

Image Acquisition Pulse Sequences

Having discussed the three dimensions of spatial encoding, it is now appropriate to assemble the encoding tasks into a single sequence of events that will yield data that can be reconstructed into viewable images. For the purpose of simplification, the discussion of spatial encoding did not take into account the dephasing effect of gradient application. This dephasing will now be dealt with, and the solution to gradient dephasing involves, not surprisingly, additional gradients. To begin with, we will construct a gradient echo sequence. This is the

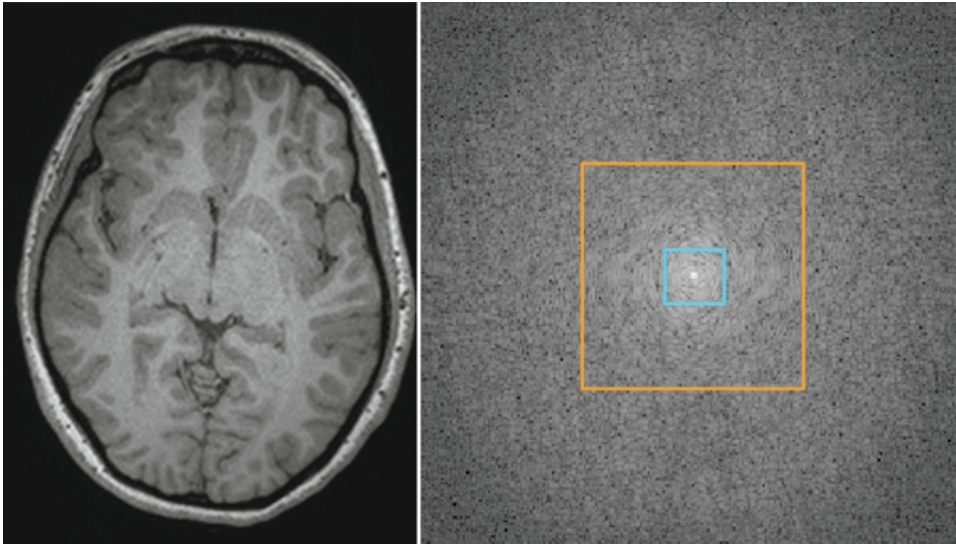


Fig. 2.10 Distribution of signal energy in k -space. *Left*: Brain image and *Right*: Fourier transform of the brain image. Most signal energy is near the center (*blue box*) corresponding to low spatial frequencies (large features and contrast). Higher spatial frequency information (*orange box*) defines edges and fine detail

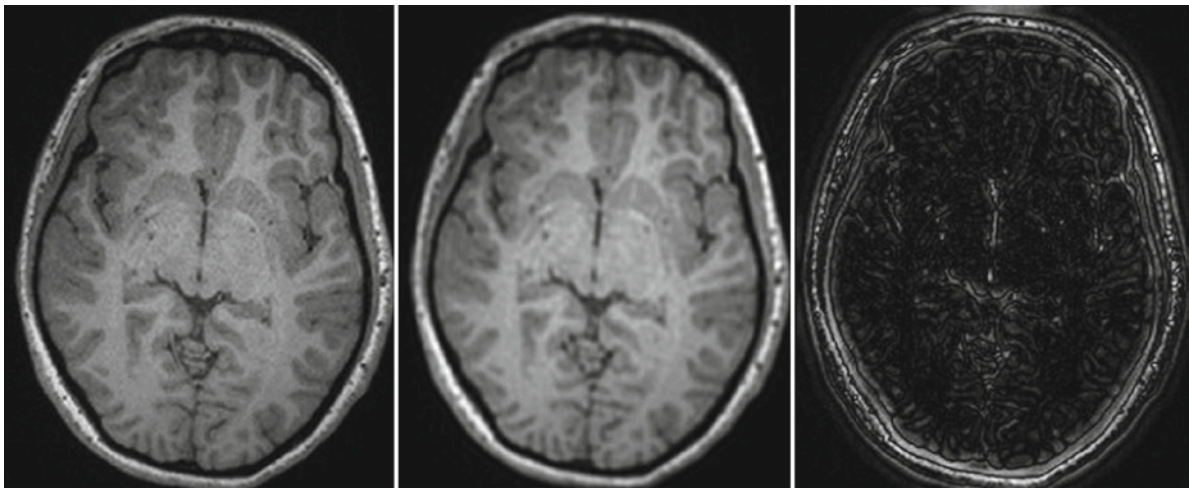


Fig. 2.11 Effect of altering k -space content. *Left*: Acquired full k -space brain image. *Center*: Blurring effect of removing outer 60% of k -space data. *Right*: Effect of removing inner 12% of k -space data (essentially a high pass filter leaving mostly edge information)

simplest sequence and it is used to generate images with T_1 and/or T_2^* contrast. Beginning with slice selection (Fig. 2.12), it was shown that the delivery of a frequency selective excitation in the presence of a gradient allows for excitation of a designated slab. It is now necessary to take into account the fact that the slice selection gradient also dephases the transverse magnetization. The solution to this problem is the application of a second gradient pulse, opposite in polarity to, and half the duration of the slice select pulse (assuming the same

amplitude but opposite polarity). The effect of this pulse is to undo the dephasing that took place during the slice select excitation. Note that the duration of the slice rephasing gradient can be reduced by increasing its amplitude. The important condition is that the area under the gradient waveform (its integral) be half that of the slice select gradient.

Next we will add the phase encode gradient. In Fig. 2.12, the phase encode gradient is shown as occurring in the same time interval as the slice rephase gradient.

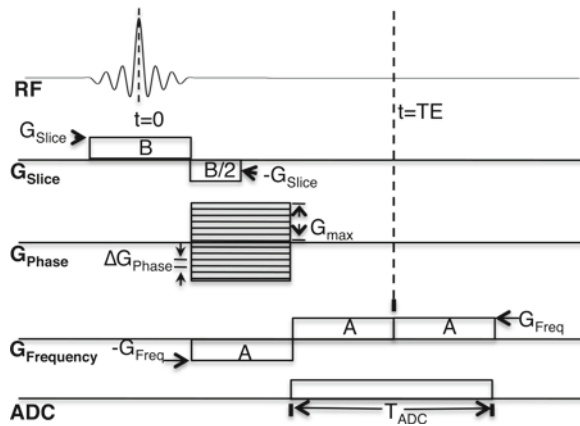


Fig. 2.12 Gradient echo pulse sequence. Following slice selection, the slice rephase, phase encode, and read rephase gradients occur in the same time interval since these activities are mutually orthogonal. The phase encode increment (ΔG_p) is given by (2.17)

This is valid because the two gradients are orthogonal. They do not have any mutual effect. In the diagram, the horizontal bars indicate that the phase encode gradient amplitude is incremented on successive repetitions of the sequence by an amount given by (2.17). For example, if a 256^2 image is being acquired, there will be 256 repetitions of the sequence, each with a different value of the phase encode gradient (other pulses remain unchanged). There is no rephase gradient associated with the phase encode gradient in the basic gradient echo sequence.

The remaining function is frequency encoding. This gradient also requires a rephase gradient, and it is placed before the encoding gradient, in the same time interval containing the slice rephase and phase encode gradients. As with the slice select rephase, the frequency encode rephase gradient is opposite in polarity to the frequency encode gradient, and the integral under the waveform is 1/2 that of the frequency encode gradient. Again, this placement is valid since the gradients are orthogonal and there is no mutual interaction. The benefit to placing these three functions into the same time interval is that the minimum achievable echo time (TE) is reduced over the case where the gradient pulses occur consecutively. This reduction in sequence execution time also allows for a reduction in the minimum achievable repetition time (TR) and for improved immunity to motion artifacts. Finally, the read gradient is turned on, along with the receiver in order to capture

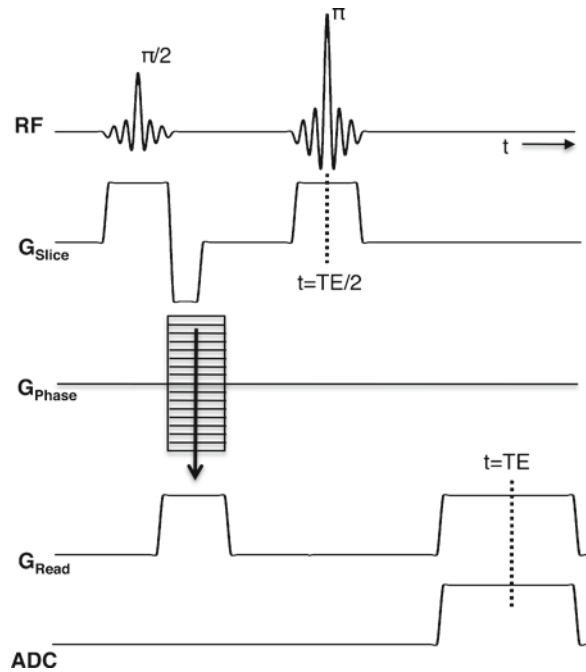


Fig. 2.13 Spin echo sequence. The 180° refocusing pulse reverses the temporal arrangement of the individual spin vectors as shown in Fig. 2.4, resulting in the formation of an echo whose peak intensity arrives at $t=TE$, which is twice the interval between the 90° and 180° pulses. The frequency encode rephasing pulse is of the same polarity as the frequency encode gradient itself due to the presence of the 180° RF pulse

the signal. The sequence is referred to as a gradient echo (or gradient refocused echo) since the frequency encode rephase gradient is used to prepare the transverse magnetization to be refocused by the frequency encode gradient. This differs from the spin echo sequence that uses a 180° RF pulse to refocus spins to produce an echo. A significant difference between the two is that the spin echo sequence removes the effect of static field inhomogeneity, and this produces images that are contrast weighted according to T_2 . The gradient echo sequence does not eliminate the effects of static field inhomogeneity (the echo is produced by gradient polarity switching) and produces images that are contrast weighted according to T_2^* . These contrast weightings assume that $TR \gg T_1$ so that there is no T_1 contribution to the result. By reducing TR, some T_1 character can be imparted to the contrast.

The spin echo sequence adds a 180° pulse for echo formation. In Fig. 2.13, it is seen that this pulse is also slice selective in order to excite the same material as

excited by the 90° pulse. Note that there is no rephase gradient. Since a 180° excitation undoes the dephasing effect of static field inhomogeneities, it also undoes the dephasing effect of its own slice select gradient. Optionally, the slice selective 180° excitation can be centered between two gradient pulses of equal amplitude and same polarity. These gradients (sometimes called “primer-crusher” gradients) spoil undesired transverse magnetization produced as a result of the imperfect slice profile (discussed previously) as well as that resulting from slight variations in the actual flip angle of the 180° excitation across the FOV. Both the spin echo and the gradient echo sequences can be preceded by a saturation or inversion pulse for the production of contrast weighted by T_1 .

A third pulse sequence is a variation on the gradient echo and is designed for rapid image acquisition. It is known as the echo-planar method and it is the most common technique used for image acquisition in brain fMRI studies. The echo-planar imaging (EPI) method can acquire all the information needed for image formation using a single RF excitation. For a given level of gradient performance, the matrix size limit (number of phase encode lines) is limited by the T_2^* of the tissue (since this is a variation on the gradient echo acquisition). The basic idea is to take advantage of the ability to refocus echoes by reversing frequency encode gradient polarity (as seen in the gradient echo). Figure 2.14 shows a pulse sequence diagram for a basic EPI acquisition. Slice selection takes place with the sequences mentioned previously. The frequency encode gradient starts with the rephase pulse as seen with the gradient and spin echo sequences. In EPI, the frequency encode gradient is then repeatedly switched in polarity to produce a string of echoes. The receiver is turned on for the entire readout duration. On the phase encode channel, a gradient pulse positions the acquisition at the end line of k -space. As the frequency encode gradient is switched, the phase encode gradient is pulsed very briefly to advance the phase to the next line to be acquired. The frequency encode and phase encode processes continue until the specified number of lines have been acquired. Since the frequency encode gradient is switching polarity on each line of data acquired, it is necessary to “reverse” one half of the lines prior to the Fourier transform when reconstructing EPI images. A limiting factor in the achievable spatial resolution of EPI is the T_2^* of the sample. As the string of echoes is being generated, transverse magnetization is decaying

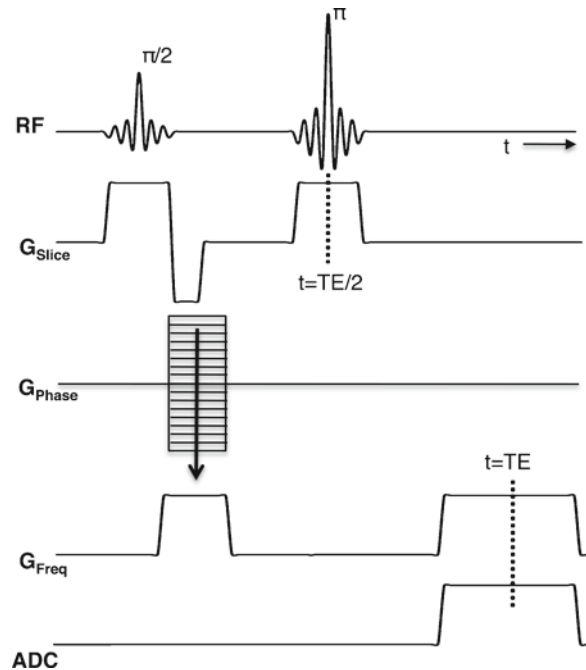


Fig. 2.14 Echo-planar sequence. Following a single RF pulse, reversals of the read gradient polarity refocus echoes. Short phase encode pulses are used to advance lines through k -space as shown in Fig. 2.9

according to the T_2^* of the tissue. If the sequence execution time is, for example, longer than $2T_2^*$, the echoes acquired at the end of the sequence will have very little amplitude compared with the echoes taken near the start of the sequence and will not contribute anything of significance to the image information. In other words, that part of k -space will have very little amplitude, and it will be as if a filter were applied to the data. For this reason, single-shot EPI acquisitions typically use matrix sizes of 64^2 – 128^2 . Of particular concern for brain fMRI imaging is a requirement that the effective echo time of the acquisition (the point where the $k=0$ and nearby lines are acquired) be approximately equal to the T_2^* of grey matter, which is approximately 30 ms at 3 T. Use of this echo time maximizes the contrast effect produced by blood flow and deoxyhemoglobin changes associated with (and occurring subsequent to) cerebral activation. Single-shot EPI resolution is significantly less than that is obtained using conventional gradient echo or spin echo structural imaging where matrix sizes of 256^2 – 512^2 are common. Multiple-shot EPI acquisitions are possible, where a different segment of k -space is sampled on

each acquisition in order to increase the matrix size (and spatial resolution) but motion effects produce artifacts when the individual groups of lines are combined for reconstruction (correction methods are available for reducing such artifacts). Multiple-shot acquisitions also reduce the temporal resolution for fMRI time series imaging protocols since multiple repetition time intervals are needed to form one image frame.

For the imaging sequences just described, it is not unusual to have TR much longer than the time required to execute the sequence. This allows for interleaved slice acquisition. Rather than acquire all the image information for one slice before moving on to the next, a number of sequence executions can take place in the TR interval in which each individual sequence execution uses a different slice selection frequency offset to excite individual slices. For example, if 12 ms are required to execute a gradient echo sequence, and the TR is 1,000 ms, it is possible to execute the sequence 83 times, with each execution exciting and retrieving information from a different slice (by changing the RF pulse frequency offset). By this means, one can acquire image data for 83 slices in the same amount of time required for the acquisition of a single slice. To minimize any “crosstalk” effects resulting from imperfect slice profiles, the slices can be acquired in such a manner that the odd numbered slices (1,3,5,...) are acquired in the first half of the TR interval, then the even numbered slices (2,4,6,...) in the second half.

It is also possible to use phase encoding in the slice direction. This is done with so-called 3D acquisitions. Slice phase encoding is done by using a non-selective RF excitation (or excitation of a wide slab corresponding to the entire stack of slices desired). The RF excitation is then followed by a phase encode gradient in the slice direction. For a gradient echo sequence, this slice phase encoding takes place in the same time interval as the in-plane phase encoding and frequency encode rephase gradients. A significant advantage to these acquisitions is the ability to generate very thin slices, typically thinner than possible using conventional slice selection methods due to gradient strength limits. With 3D acquisitions, it is possible to generate image datasets with isotropic resolution (slice thickness equal to the in-plane resolution) of better than 1 mm for whole-head scans. A caveat is that since the slice direction is phase encoded, there must not be any tissue outside of the volume to be imaged in the slice direction or else aliasing will result. Another caveat is that these acquisitions can

be lengthy if TR is not very short. Contrast preparations can be used with 3D sequences by segmenting the acquisition of k -space data. An advantage for isotropic resolution datasets is that a single acquisition can be reformatted for viewing in different orientations. For example, a dataset acquired in the transverse orientation can be easily reformatted for viewing as sagittal or coronal images.

Contrast

MRI has the ability to generate contrast between many types of soft tissue without the need for contrast agents. Generally, this is done by exploiting differing T_1 , T_2 , and T_2^* values between tissue types. For anatomic (structural) imaging of the brain, the materials of interest are grey matter, white matter, and CSF. Table 2.1 shows the approximate relaxation time constants for brain^{10–18}:

At 3 T, it is seen that the percent difference in T_1 for grey and white matter is greater than that for T_2 . For generating contrast between grey and white matter, it is preferable to generate contrast by using sequences with T_1 contrast weighting. This approach also allows the use of minimum echo times to reduce motion sensitivity.

One mechanism for generating T_1 contrast is known as partial saturation. As mentioned in “Relaxation” section, by delivering excitation with a repetition rate $TR < 5T_1$, that longitudinal recovery will not be complete when successive excitations take place. Materials with different T_1 will recover to different degrees, and therefore the signals produced will differ in amplitude. Figure 2.15 shows a plot of signal intensity vs. TR for grey and white matter at 3 T. Taking the difference between the two curves shows the TR at which the signal difference (contrast) is maximized. By acquiring a gradient echo image at that value of TR, a T_1 weighted image will be produced. In this case, the echo time (TE) is set to the shortest possible value in order to

Table 2.1 Approximate Relaxation Time Constants for Brain at 1.5 T and 3 T

Tissue	T_1 1.5 T	T_2 1.5 T	T_1 3 T	T_2 3 T
Grey	1,090	100	1,400	80
White	630	70	805	50
CSF	3,840	2,600	4,200	3,000

minimize T_2^* contribution to the contrast. As seen in the left image of Fig. 2.16, there is contrast between the grey and white matter.

It is possible, however, to improve the level of contrast over that available using partial saturation. As discussed in “Relaxation” section, the T_1 of a sample can be measured using inversion recovery. This involved placing a 180° (inversion) excitation and delay in front of a signal readout pulse. Such a process can also be used for imaging. In this case, the 180° excitation and delay can be placed in front of a gradient echo sequence. One can even set the inversion recovery delay (TI) to

null either grey or white matter, which can be considered the ultimate in contrast. As shown in (2.10), the value of TI required to null signal from a tissue is also influenced by the selection of TR. Inversion recovery is the preferred method for generating grey–white contrast in structural brain imaging. It is also possible to generate T_1 contrast using a 90° excitation in front of the image readout. This is known as saturation recovery. Inversion recovery, however, doubles the dynamic range ($-M_0 \rightarrow M_0$) of the longitudinal magnetization over saturation recovery ($0 \rightarrow M_0$) and therefore produces more contrast (Fig. 2.16), and allows for the nulling of one component based on its T_1 if desired.

T_2 contrast weighting is also of use in brain imaging. Note that from Table 2.1 it is seen that there is a very substantial difference between the T_2 of CSF and those of grey and white matter. This is a consequence of CSF consisting largely of free water. The small mobile water molecules experience considerable motion, such that the interactions between neighboring magnetic dipoles are more completely randomized and cancel to a greater degree than for less mobile molecules, resulting in a very long T_2 compared with tissue water, which is much less mobile and therefore subject to greater dephasing effects. T_2 contrast is generated using the spin echo sequence, which has the ability to cancel effects due to \mathbf{B}_0 inhomogeneity, leaving only the true T_2 decay of the signal. In this case, one sets the TE based on the maximum difference between the signal curves (signal vs. TE) based on the T_2 values to be distinguished. In the case of CSF, a long echo time, typically 100–200 ms, will be used such that some tissue

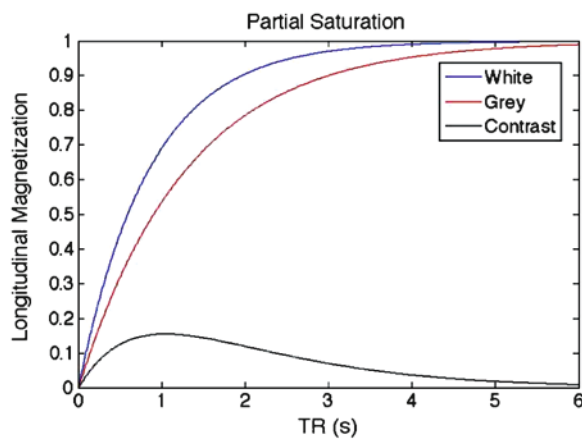


Fig. 2.15 Partial saturation signal intensity vs. TR for grey and white matter at 3 T. Also shown is the difference signal, which reaches its maximum at $\text{TR} \approx 1,000$ ms. This TR value will produce the maximum grey–white contrast for a partial saturation acquisition

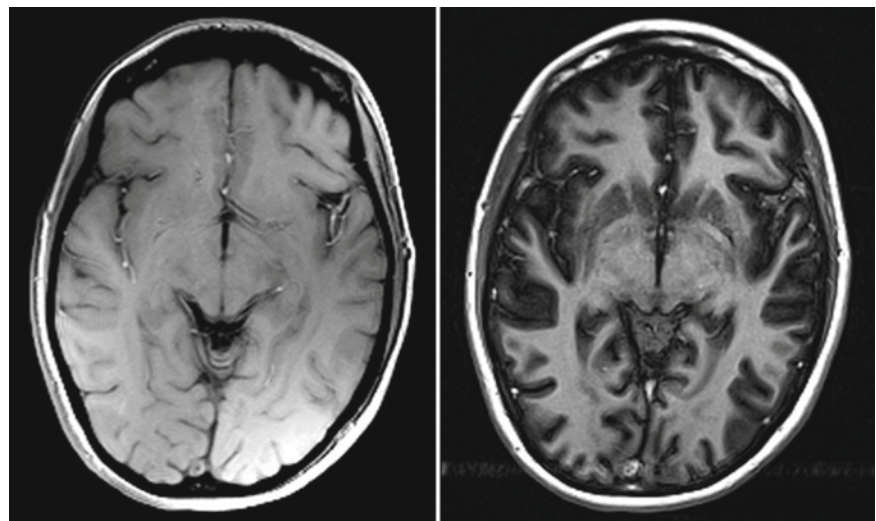


Fig. 2.16 Contrast examples at 3 T: partial saturation with $\text{TR} = 1,000$ ms gives grey–white contrast. *Right:* Inversion recovery produces substantially more contrast between grey and white matter

signal remains for reference purposes, and the CSF compartments return high signal intensity. This sensitivity to free water makes T_2 contrast a preferred

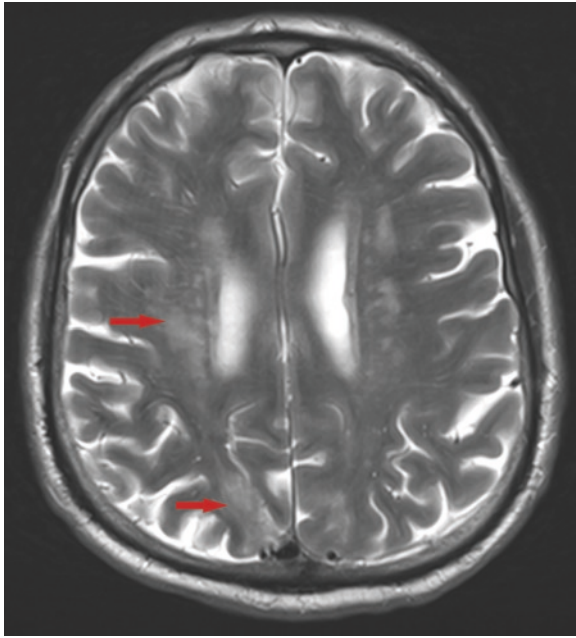


Fig. 2.17 T_2 contrast weighting. Example of poststroke acquisition showing regions of edema (arrows) as increased signal intensity resulting from increased extracellular water

method for imaging following stroke, where regions of edema (accumulation of extracellular water) will return higher signal intensity than normal tissue (Fig. 2.17).

It is also possible to generate contrast based on T_2^* . This is done using a gradient echo or echo-planar sequence with a suitable TE. As indicated in “Relaxation” section, the gradient echo does not compensate for the effects of static field (B_0) inhomogeneity. T_2^* weighted sequences are therefore useful for examining tissues where susceptibility gradients on a small scale can exist, for example, from iron deposition in tissue. Brain fMRI scanning is done using T_2^* weighted sequences since the objective is to be sensitive to blood oxygenation changes, and the magnetic susceptibility of oxyhemoglobin is less than that of deoxyhemoglobin. A caveat regarding T_2^* weighting relates to the range of echo times that are feasible. Increasing TE increases the sensitivity of the sequence to B_0 inhomogeneity – any inhomogeneity, whether it arises from tissue structure on a small scale, or from large susceptibility gradients that result from air–tissue interfaces as seen with the orbitofrontal cortex (which borders the sinuses), or from inhomogeneity resulting from field shim errors. Long echo times in the presence of such inhomogeneities results in geometric distortion or even signal loss as shown in Fig. 2.18.

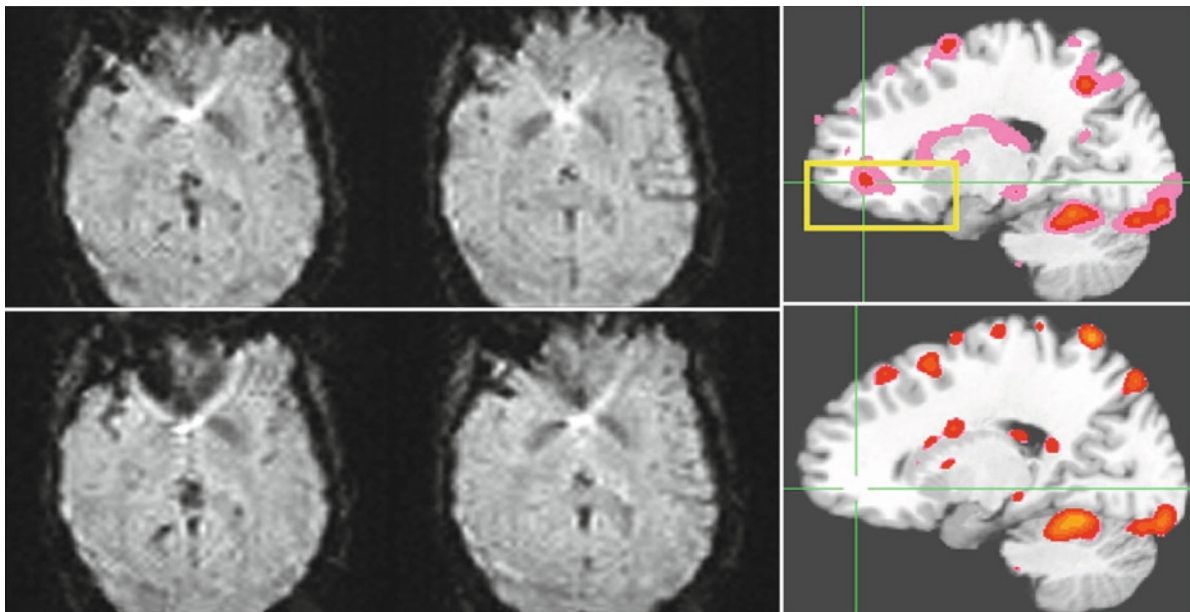


Fig. 2.18 Echo-planar image examples from the orbitofrontal cortex showing the effect of the air–tissue susceptibility difference. *Top*: Images acquired using a localized shim on the orbitofrontal cortex. *Bottom*: Same data acquired using the default shim

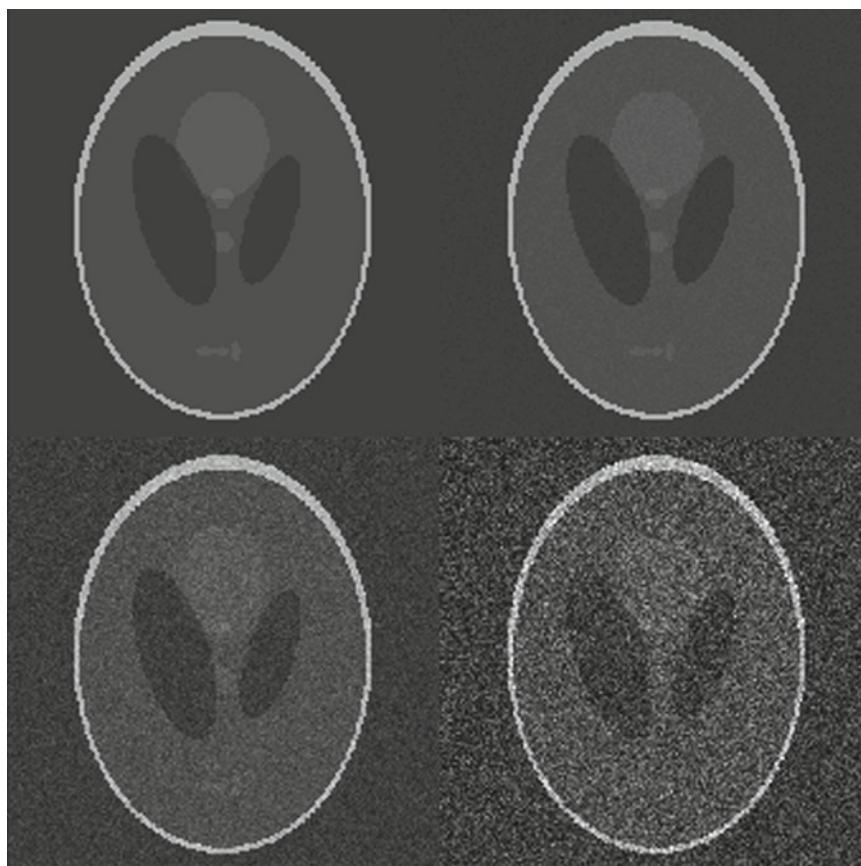
condition. In the default shim case, there is substantial signal loss in the orbitofrontal cortex. Localized shimming restores intensity. F-statistic maps on the *right* show activation data that was not seen with the default shim

MRI is also capable of generating images with contrast weighting based on some aspects of physiologic function. For example, maps of flow velocity can be generated using a sequence in which gradient pulses will produce phase shifts in flowing spins, as compared to stationary spins.^{19, 20} Using expressions relating flow velocity to phase shift, it is possible to build maps of flow velocity in arteries and veins, which is helpful in assessing vessel patency and determining total blood flow to specific regions. Of particular relevance to neuroimaging studies are the fMRI techniques for detecting hemodynamic events relating to cerebral activation (Chap. 4), diffusion weighted and diffusion tensor imaging (Chap. 5), and quantitative perfusion imaging (Chap. 6). Magnetic resonance can also be used for producing information related to the presence of specific metabolites, using spectroscopic techniques. In fact, for most of the history of use of the magnetic resonance phenomenon, analytic spectroscopy has been the primary application.

Signal-to-Noise Ratio

In order to distinguish structures, it is necessary to have contrast. It is also necessary that the contrast be distinguishable in the presence of noise. Noise will be a factor in any measurement and is a form of uncertainty in the measured parameter. Noise arises from random electron motion in the receiver electronics, RF coils, and the subject. This noise is characterized by having equal power at all frequencies within the receiver bandwidth, and is sometimes referred to as white noise. White noise appears in images as a uniform speckling with no distinguishable texture (Fig. 2.19). The effect of improving signal-to-noise ratio (SNR) is to reduce the magnitude of speckling and improve the ability to distinguish small differences in signal intensity between different structures or to visualize fine detail. The variance of noise is proportional to temperature, the resistance of the loaded RF

Fig. 2.19 Simulated head phantom images with varying degrees of noise: Noise-free (upper left), SNR = 50 (upper right), SNR = 10 (lower left), and SNR = 4 (lower right). Ability to observe small contrast variations is compromised in the image center at SNR = 10 and the small features located at the lower center of the image are essentially lost at SNR = 4. SNR values are referenced to the bright border of the “head”



coil, and the receiver bandwidth. The receiver bandwidth is the one factor in this relationship over which the scanner operator (or sequence programmer) can exercise some control.

As seen in Fig. 2.19, noise can overwhelm small contrast variations, compromising the ability to make a diagnosis or to extract a quantitative parameter from images. There are a number of relationships that exist between scan parameters and SNR that can be varied in order to generate images with adequate SNR for a particular purpose. SNR varies with these parameters:

1. Voxel size (linear dependence)
2. Repetition time (monoexponential dependence according to T_1)
3. Echo time (monoexponential dependence according to T_2 or T_2^*)
4. Flip angle (interactive dependence with repetition time and T_1)
5. Receiver bandwidth (square root dependence)
6. Choice of resonator (linear dependence with fill factor which is the ratio of the volume of excited tissue to the volume of the resonator)

Voxel size is determined by the slice thickness and the in-plane resolution. Higher-resolution images not only require more time for acquisition, but for all other parameters fixed, they will also have reduced SNR. Voxel size is the product of the two in-plane pixel dimensions and the slice thickness. For example, doubling the slice thickness will double the SNR, but this change must be weighed against the effect of additional partial volume effects due to the additional anatomy contained in the larger slice.

As shown in the example in Fig. 2.15, increasing TR increases the available signal in a partial saturation acquisition. This change must be weighed against the effect on contrast. For grey and white matter, optimum contrast was achieved with a TR of about 1 s. The critical factor for distinguishing two structures from each other is the contrast-to-noise ratio (CNR), which is the ratio of the signal difference between two structures and the noise. For most situations, these tradeoffs have been determined by the scanner manufacturer, and optimized protocols are included in the scanner software package.

A reduction in echo time will result in greater SNR. In general, for acquisitions other than T_2 or T_2^* weighted imaging, the echo time will be set to the minimum possible value in order to maximize SNR and to minimize motion sensitivity and T_2 or T_2^* contributions

to the contrast. For most T_2 weighted imaging, the echo time will be set to retain some tissue detail while providing for a high signal from free water (CSF). For BOLD fMRI scans, the echo time will be set to the T_2^* of grey matter in order to maximize the BOLD susceptibility contrast.

Flip angle is also a contrast parameter, and its relationship to signal intensity is more complex than that for TR and TE. When TR is set to allow for complete recovery of longitudinal magnetization ($TR > 5T_1$), a flip angle of 90° will produce the largest possible signal. When operating at shorter TR values, the signal that will be obtained is a function of the flip angle, the TR, and the T_1 of the tissue in question. For a basic gradient echo acquisition, the signal dependence is given by:

$$M_{xy}(\theta, TR, TE, T_1, T_2) = \frac{M_0 \sin \theta (1 - e^{-TR/T_1}) e^{-TE/T_2}}{(1 - \cos \theta) e^{-TR/T_1}} \quad (2.18)$$

For T_1 weighted imaging, the TE will be set to the shortest possible value, and the last term in the numerator becomes negligible. For maximizing SNR for a structure of known T_1 , it is necessary, for a given TR, to determine the flip angle giving the largest signal. This flip angle is known as the Ernst angle, and is given by:

$$\theta_E = \arccos(e^{-TR/T_1}) \quad (2.19)$$

For rapid gradient echo imaging, where TR values can be on the order of 7 ms, the Ernst angle for grey matter at 3 T will be approximately 6° . Using (2.19), the signal intensity for $TR = 7$ ms and $\theta = 6^\circ$ from grey matter will be $0.096 M_0$. While this represents the largest signal that can be obtained from grey matter for a TR of 7 ms, it is clear that the contrast available will be meager, and the SNR will likely be poor. The preferred approach for generating rapid T_1 weighted images, therefore, is to use contrast preparation, typically inversion recovery, and then use a segmented rapid gradient echo readout to obtain the spatially encoded data.

Receiver bandwidth affects SNR with a square root dependence. Doubling the receiver bandwidth results in a factor of $\sqrt{2}$ reduction in SNR. Receiver bandwidth setting is generally transparent to the user, although it is generally possible to drop into a lower-level menu for setting such system parameters. Receiver bandwidth (BW) is a function of the signal sampling time per point (Δt), and the faster the data is sampled, the wider the receiver bandwidth will be:

$$BW = \frac{2}{\Delta t} \quad (2.20)$$

The tradeoff here is sampling rate vs. time required to read a line of data. Longer sampling time results in smaller bandwidth and improved SNR. However, longer sampling time per point results in a longer frequency encode interval, which increases the minimum echo time. For rapid gradient echo imaging, this also implies a longer minimum TR and longer scan time. Longer echo time also translates into increased motion sensitivity and increased susceptibility artifact. Generally, these tradeoffs have been taken into account in the design of the default protocols provided as part of the scanner's software package. Specific circumstances might dictate deviation from default bandwidth settings when the shortest echo time possible is needed (e.g., presence of strong susceptibility gradients) or if getting all the possible SNR available becomes critical (e.g., arterial spin labeled perfusion imaging).

For resonators, the general practice is to use the one that provides the best fill factor for the anatomy to be scanned. For heads, array receive resonators are now commonly used. In some cases, when a specific grey matter region is to be scanned (e.g., occipital cortex for visual studies involving V_1 and V_2), an array surface resonator may be used. As the name implies, this resonator is placed directly on the surface of the head, and will return a large signal from the tissue directly underneath. For scans not requiring whole-brain data, surface resonators provide a means of gaining a substantial improvement in the effective fill factor over a whole-head volume resonator for cortical imaging.

A common method for improving SNR is signal averaging. This is the acquisition of the same image data two or more times, with the data summed (or averaged, the difference is only a scaling factor). Since the signal adds linearly, and the noise adds with a square root dependence, the SNR improves by a factor equal to the square root of the number of acquisitions. Acquiring the same image data four times and summing results in a doubling of the SNR. Since the scan time increases linearly with the number of averages, scan time and patient tolerance must be taken into consideration when using averaging. For example, to double the SNR of a 4 min acquisition using averaging, four acquisitions will be necessary, totaling 16 min. Motion correction may be necessary if the data were acquired as successive complete scans.

MRI Hardware

The Magnet

With an understanding of the imaging process, it is useful to examine the machinery that brings it all about. The most obvious component of an MRI scanner is the magnet that produces the static field (B_0). In most cases, this is a superconducting solenoidal design in which the main field is produced within a cylindrical bore. The superconducting design possesses some important advantages. A very uniform field can be produced over a DSV on the order of 50 cm, allowing for coverage of a large FOV in a single acquisition. The magnet does not require a constant input of electric current, as would be required with a conventional resistive electromagnet. Superconductivity implies that there is no heat generated as a result of resistive losses in the field windings. Once a superconducting magnet has been energized, the current in the field windings circulates indefinitely (for all practical purposes) with no further input of energy. There is a loss of current over a very long time scale due to electron-electron interactions, but these do not influence the routine operation of the system. The disadvantage of superconducting systems relates to the cost of cryogenics required to maintain the superconductivity of the field windings. The niobium-titanium alloy typically used in this application has a critical temperature of about 11.7 K, below which the alloy is superconducting. In order to maintain the field windings below the critical temperature, they are immersed in liquid helium, which has a boiling point of 4.2 K. Older magnets enclosed the liquid He vessel inside another filled with liquid nitrogen (boiling point 77 K) to limit heat transfer from the environment to the He vessel. The housing containing the cryogen vessels is pumped down to a vacuum to eliminate air as a heat transfer medium. Newer magnet designs eliminate the nitrogen vessel, and have reduced the He fill interval compared with the original generation of clinical scanners. The development of an alloy that would be reliably superconducting at liquid nitrogen temperature would be very welcome, in that liquid nitrogen is inexpensive and is also much easier to handle. The field winding set consists of multiple elements. These are designed to increase the size of the most uniform part of the field (variation of a few ppm) to permit imaging at a FOV as

large as 50 cm (centered on isocenter) in all possible tomographic planes. When a new scanner is delivered, it is first cooled by repeated fillings with liquid He. Once the magnet temperature is stabilized, it is brought up to field using a power supply connected to the main field windings through a superconducting switch. In a manner resembling the charging of a battery, current is added to the system over a period of a few hours until the main field winding is carrying the current required to generate the specified B_0 . At this point, the superconducting switch is closed, and the current in the field windings continues to circulate. There will be a slight reduction in the field winding current over the next 24 h or so after which it stabilizes, at which point the field strength is measured by measuring the resonant frequency (2.1). Once the field strength and stability are confirmed, a shimming process takes place to further improve the uniformity of the field over the imaging volume. This is done following placement of the gradient set and whole-body RF coil. This process takes into account imperfections in the field windings as well as interactions from nearby metal structures. On some magnet designs, this involves adjusting the current in a set of superconducting shim windings. Other designs use a passive method in which metal plates of various size are placed in holders that line the bore of the magnet. A field map sequence is executed with results fed to a program that instructs the service engineer regarding the placement of plates with respect to quantity and location.

Permanent magnet-based “open” designs are also available. These tend to be of lower field strength (typically 0.35 T) and the less uniform static field limits the usable FOV. The SNR and susceptibility contrast implications of the lower field strength and the gradient performance available do not render permanent magnet systems as the first choice for functional neuroimaging applications. Permanent magnet systems do possess two advantages over superconducting systems: no cryogenics are used and the open design is more easily tolerated by claustrophobic patients.

The Gradient System

Spatial encoding of the MR signals is accomplished through the use of linear magnetic field gradients. These linear gradient fields are superimposed on the static

magnetic field and are switched on and off as necessary to accomplish image acquisition as described in the section on image acquisition pulse sequences. The gradient system consists of two major components: the gradient field windings and the gradient amplifiers.

To provide for three-dimensional spatial encoding, it is necessary to produce linear field gradients in three directions corresponding to the orthogonal axes of the spatial reference frame. For MR imaging, these are defined as the z -direction (along the bore of the magnet) and the x,y -directions (horizontal and vertical). For each of these directions, a set of field coils are provided that will produce a linear field gradient when current is passed through the coil. These coils are resistive (not superconducting) and only produce gradient fields when current is sent through them. Resistive coils are necessary since imaging sequences require that the gradients fluctuate quickly.

Gradient amplifiers are used to produce the large current pulses that are required to drive the gradient coils. These currents will be in the range of hundreds of amperes. Typical maximum gradient strengths now exceed 40 mT/m in clinical systems, with gradient slew rates as high as 200 T/m/s. For a given gradient coil, the strength of the gradient field is linearly proportional to the current flowing through the coil. Gradient strength has implications with respect to the speed of imaging. Strength also influences minimum echo times and time required, for example, for diffusion encoding. Another important factor, especially for echo-planar fMRI is the slew rate (or ramp time) that is achievable in a given gradient system. The greater the maximum slew rate, the less time is required for the gradient field to reach its assigned strength (and to be changed or switched off). Maximum slew rate is a function of the characteristics of both the gradient coils and of the amplifiers. Any conductor has an associated inductance (L) and since $V = L(dI/dt)$ where V is the amplifier output voltage and dI/dt is the rate of current change (slew rate), it is seen that the greater the maximum output voltage of the amplifier, the greater the slew rate will be. Alternatively, reducing the inductance of the gradient coil will also increase the slew rate for a given applied voltage.

Increasing gradient slew rates allows reduction in the echo time (TE) of both gradient echo and spin echo acquisitions (not to mention echo-planar and spiral scan techniques^{21, 22}). Unless the objective is a deliberately long echo time for T_2 or T_2^* contrast weighting,

reducing the minimum TE brings some important benefits:

1. Greater immunity to motion artifacts relating to blood and CSF pulsatility.
2. Reduced artifacts arising from susceptibility gradients, very important in the orbitofrontal cortex.
3. Reduced signal acquisition time in EPI allowing for more slices per TR period in fMRI studies.
4. Ability to reduce repetition time (TR) in rapid gradient echo imaging for reduced imaging time in T_1 weighted anatomic structure imaging (e.g., T_1 MP-RAGE²³).

For whole-body gradients with slew rates on the order of 150–200 T/m/s concerns exist regarding peripheral neurostimulation that can result from currents induced in the body from the rapidly switching gradient field (a time varying magnetic field will induce a current in a conductor). However, for the gradient switching rates available in clinical scanners (adhering to FDA guidelines), neurostimulation is not a significant issue, and generally will not be a factor at all if the patient is advised prior to scanning.

The rapidly switching gradient fields can also induce currents in other components of the magnet. These induced currents, in turn, will generate their own gradient fields that act to degrade image quality. As with the static magnetic field, these effects can be reduced through the use of active shielding in which additional coils are used to cancel the gradient field outside of the gradient coil set. Such gradient sets involve greater purchase cost than unshielded gradient sets and require greater currents and drive voltages (owing to increased inductance). However, such gradient systems are essential for functional neuroimaging (and diffusion tensor) applications. The lifetime of induced currents in the magnet structure from unshielded gradients is typically longer than the desirable echo time desirable ($TE < 2.5$ ms) for T_1 weighted (e.g., T_1 MP-RAGE) gradient echo structural imaging.

Another specification to consider for gradient systems is the linearity. A gradient coil set is intended to produce linear gradient fields on the three spatial axes. However, this linear portion of the gradient field does not cover the full extent of the magnet bore. As mentioned previously, the isocenter of the magnet is defined as the point where the magnetic field strength does not change when a gradient is turned on. Slice offsets are defined with the isocenter as a reference (i.e., slice

offset = 0 mm). For images to appear without geometric distortion, the gradient fields must be linear throughout the region defined for the tomographic plane to be acquired. If this is not done, any anatomy outside of the linear region of the gradient set will be rendered with geometric distortion. For clinical scanners, a typical linearity specification would permit the use of FOV settings as large as 50 cm. Over this volume, the gradient linearity is at least 95% (typical specification). For imaging heads, this volume is more than adequate.

During operation, the gradient coil set can produce a considerable sound pressure level. When a current is passed through a conductor that is in a magnetic field, the conductor will experience a force. This principle is exploited in the design of electric motors. In a clinical scanner, the large static magnetic field, combined with the high currents and rapid switching used for the gradient pulses, results in large forces generated in the gradient conductors, with resulting sound. The characteristic sounds produced are a function of the type of imaging sequence, the repetition and echo times, number of slices, etc. Higher slew rates generally correspond to greater loudness. Patients are provided with hearing protection during studies, typically in the form of disposable ear plugs.

RF Coils

The RF coil, also referred to as a resonator, acts as the antenna for transmission of the RF excitation (B_1) and for reception of the resulting MR signals. Although an antenna is typically thought of as a device intended to transmit a radiofrequency field away from the transmitter site, an RF coil for MR imaging is designed to confine the RF magnetic field to the imaged volume. At the same time, this RF field is intended to be as uniform in intensity as possible over the imaging volume. Coils fall into two classes: volume coils and surface coils (with a further subdivision known as array coils for both classes). In all cases, the RF coils are resonant circuits, intended for operation at a specific (Larmor) frequency (although some coils permit operation at two frequencies for spectroscopy). A resonant coil develops stronger transmit fields (for a given transmit power) and is capable of receiving weaker signal strengths than a non-resonant device. In addition, the frequency selectivity (bandwidth) of the coil improves

receive SNR by imposing an additional degree of selectivity to the receive system. For imaging, coils are resonant at the proton (^1H) frequency of the scanner. On a 1.5 T system, this is approximately 63 MHz, for 3 T, approximately 128 MHz. Most scanners are equipped with a large volume coil (generally referred to as the body coil) that actually forms the innermost “layer” of the scanner bore (it is located inside the gradient set). This coil has an inner lining and is not visible to the patient. A common configuration for volume coils is the “birdcage” configuration (Fig. 2.20). In this design, one or two legs are driven, with the remainder acting as passive radiators such that a uniform radiofrequency field is produced within most of the volume of the coil. The inner diameter of the body coil actually defines the usable diameter of the scanner bore. Although a magnet may have a 90–100 cm bore, once the gradient and shim coil sets, and the body RF coil are inserted, the remaining diameter available to accommodate the patient will be on the order of 55–70 cm. The body coil is intended to produce an adequately uniform RF field over a volume corresponding approximately to the linear region of the gradient set. The most basic mode of operation for the

body coil is the one in which it is used for both transmit and receive. This is a convenient mode of operation, especially for scout imaging in which a large volume is to be imaged quickly for purposes of identifying the regions of interest and establishing tomographic planes for detailed study. In general, the larger the coil, the greater the transmit power required to produce a given flip angle in the region of interest. Thus, the body coil requires more transmit power than the other coils used on a clinical scanner. For the 180° pulses required for spin echo imaging, several kilowatts peak power can be needed in order to permit the use of adequately short RF pulses.

The SNR of an image depends (among other factors) on the fill factor. The fill factor is defined as the ratio of the volume of tissue excited to the sensitive volume of the coil. Typically, the ratio of the volume of a tomographic slice to the sensitive volume of the body coil is very small. In order to improve the SNR for specific studies and to permit the use of smaller FOV settings, smaller volume coils and surface coils are employed. For brain imaging, a head coil is routinely used. As the name suggests, head coils are designed to accommodate a head only. The advantage is that the improved fill factor results in improved SNR over what would be achieved using the body coil for transmit and receive. Traditionally, the head coil was a transmit/receive device producing an adequately uniform B_1 field over a head. More recent scanner designs take advantage of multielement receive coils as will be discussed below.

A surface coil is placed on the body, as close as possible to the structure to be imaged. Surface coils may be used as transmit/receive antennas, or they may be used in a mode in which the body coil transmits the RF field, and the surface coil is used as the receive antenna. The latter approach has the advantage of providing a uniform transmit field, effectively improving the intensity profile of the image. The reason for this is that a surface coil produces a non-uniform field when used as a transmit coil. The field intensity falls off with distance from the plane of the surface coil. This same dependence applies to sensitivity for receiving the signal. Use of the body coil as the transmit antenna removes the spatial dependency of the transmitted RF field. The spatial dependence in the receive profile can be exploited to improve the spatial resolution of images. If the FOV of the scanner in the phase encode direction is set smaller than the size of the subject, signal from outside the

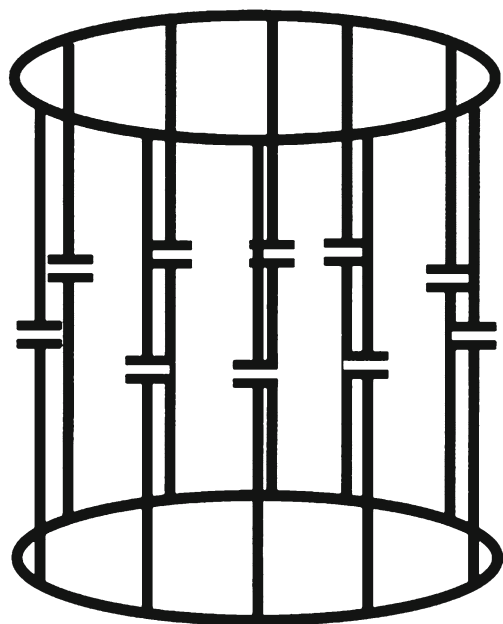


Fig. 2.20 A birdcage volume resonator consists of multiple radiating elements intended to produce a uniform B_1 distribution and receive sensitivity profile across a specified volume. Capacitors along with the inductance of the elements along with a matching network determine the resonant frequency

FOV will alias (“fold-over”) into the image. Since the surface coil will pick up signal only from its vicinity, the FOV can be set to smaller values, corresponding to the size of the surface coil without the possibility of fold-over since there is no signal arising from outside the region of interest. Since the FOV can be set smaller, for a given matrix size (e.g., 256×256), the pixel size will be smaller, and finer detail can be resolved. Surface coils contain a decoupling circuit that shifts the resonant frequency of the coil when the volume coil is transmitting in order to prevent retransmission resulting in artifacts or even RF burns.

A class of RF coils that are increasingly used in neuroimaging studies is the array coils. As the name indicates, such coils consist of multiple elements that are arranged in a housing and connected in such a manner that they can be as simple to use as a conventional coil. With some coil designs, the housing can be flexible such that the coil array can conform to the geometry of the patient. For imaging heads, volume array coils (Fig. 2.21) are available that resemble the conventional transmit/receive head coils traditionally used on clinical scanners. The purpose of array coils is to attempt to combine the best aspects of surface coils and volume coils. Surface coils are intended to produce images of improved SNR over a specific region (when compared with the same images acquired with a body coil). Volume coils provide a more uniform RF field homogeneity to provide consistent intensity and contrast across the entire FOV. A phased-array receive coil can provide receive sensitivity over a larger area (since it consists of multiple coil elements) and can rely on the body coil for a uniform transmit field. Use of array coils requires the ability to receive the individual element signals and combine them in the proper manner to produce the composite receive signal. This generally requires the use of multiple receiver channels on the scanner, with appropriate signal processing capability. Although these capabilities add to the cost of the scanner, the results justify the costs with SNR improvements of more than a factor of 2 available. Array coil capabilities have therefore become standard on scanners intended for neuroimaging applications. While some variation of signal intensity characteristic of surface coils is seen in the array coil image, the difference in SNR is readily apparent.

Array surface coils with multiple receivers permit the use of techniques to increase the speed of image acquisition. This class of parallel imaging acquisitions

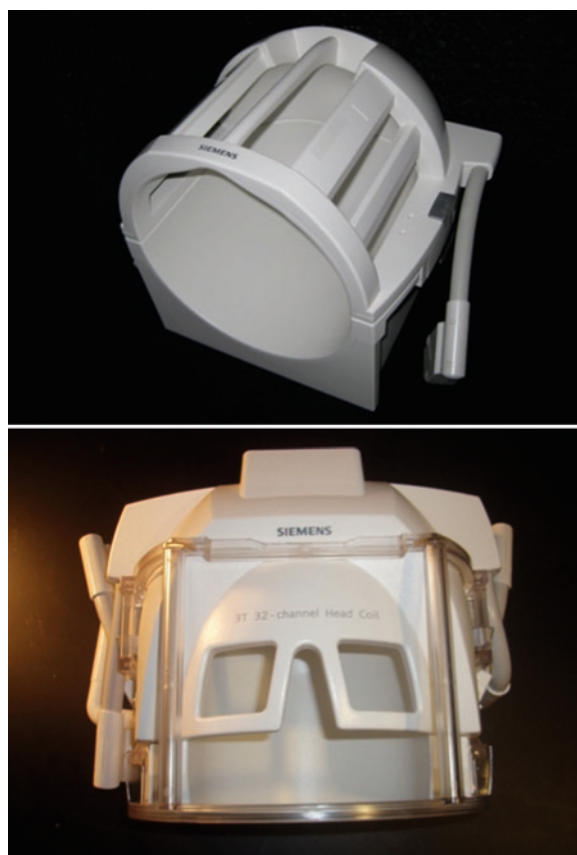


Fig. 2.21 Two examples of volume array head coils. On the *top* is a 12-channel unit with a 32-channel unit on the *below*. Preamplifiers for each channel are located at the back of the housing for improved receive signal-to-noise performance (Siemens AG Medical Solutions)

such as SMASH (Simultaneous Acquisition of Spatial Harmonics),²⁴ SENSE (Sensitivity Encoding),²⁵ UNFOLD (Unaliasing by Fourier-Encoding the Overlaps Using the Temporal Dimension, itself not a parallel method but can be combined with a parallel method),²⁶ and GRAPPA (Generalized Autocalibrating Partially Parallel Acquisition)²⁷ make use of the known sensitivity profiles of array coil elements to simultaneously acquire information corresponding to more than one k -space line at a time. With the use of appropriate postprocessing to resolve the spatial harmonics in order to produce the complete k -space representations of the images, scan time reductions on the order of two- to fourfold can be achieved, with a factor of 2 producing acceptable results for a 12-channel head coil and a factor of 4 practical for use with a 32-channel head coil. Such parallel methods can be applied to most fast

imaging methods, further multiplying the speed of these techniques without incurring an unacceptable signal-to-noise penalty. These parallel imaging methods also go by several trade names as used by the various scanner manufacturers.

Safety

Safety in MRI centers on three considerations: the static magnetic field (B_0), the radiofrequency field (B_1), and the gradient fields. Of these three considerations, the static field is the one typically associated with contraindications to MR scanning.

The static field of clinical scanners ranges from 0.35 (for some open permanent magnet systems) to 3 T (for cylindrical bore superconducting systems) and higher for some research scanners. The primary concern relates to biomedical implant devices. These consist of a wide range of geometries and materials, and include both passive and active devices (such as pacemakers and cardioverter/defibrillators). Devices are classified as MR-Safe (no danger in any MRI environment), MR-Conditional (safe at some field strengths), or MR-Unsafe (dangerous at any clinical field strengths). Standard testing procedures have been published for assessing ferromagnetic force and torque that include criteria for a Safe designation. The general criteria for the Safe designation being that a device experience no more force or torque from the magnetic field than it does from gravity. Given the extent of tissue damage that can result from implant device migration due to ferromagnetic force or torque, it is essential that the manufacturer and specific model of implant device in a patient be unambiguously determined. This information should be available in the medical records, and publications exist that allow an MRI technician to confirm the MR safety status of a given implant device. If any doubt exists regarding the identity of an implanted device, the patient enclosing the device should not be scanned. A technician will typically go over a screening form listing contraindications to imaging with each patient to be scanned to insure that the questions are clearly understood, especially with regard to implanted devices or residual metal fragments from a previous injury.

Safety concerns extend to any equipment to be brought into the scanner room. MRI compatible

medical equipment (e.g., monitoring devices, IV poles, oxygen tanks, etc.) is available and should be clearly marked regarding their safety status. If there are any doubts, a handheld magnet can be kept at the scanner facility for testing questionable items for ferromagnetic force development.

There are safety issues relating to the B_1 field as well. These all relate to radiofrequency energy absorption by tissue, over a large volume, or on a very localized basis. Radiofrequency energy absorption by tissue results in an increase in temperature, so the FDA has issued guidelines regarding the rate at which RF energy can be applied. The specific absorption rate (SAR) is expressed in units of W/kg and for the whole body averaged over 15 min, the maximum SAR is 4 W/kg. For heads, the limit over 10 min is 3 W/kg. When scan parameters are being set, an estimation of the SAR is provided to the operator. Excessive SAR values will require modification of one or more scan parameters. For example, increase in TR (to reduce deposition rate) or reduction in flip angle (to reduce RF transmit power). Rapid spin echo sequences are of particular concern due to the extensive use of 180° pulses over short time intervals. Higher flip angles correspond to stronger B_1 fields, which in turn correspond to higher RF transmit powers. RF absorption increases with frequency, so the SAR issue becomes more prominent as main field strength (B_0) increases.

SAR is influenced by scan type and parameters, and affects all the tissue within the usable volume of the transmit coil. There exist RF safety issues of a more focal nature. One relates to the use of surface coils. During volume coil transmit, the surface coil is deliberately detuned (a user-transparent process) to move its resonant frequency away from the Larmor frequency. If this were not done, a very strong RF current would be induced in the surface coil, with resultant retransmission of an intense RF field by the surface coil. This retransmitted field can be strong enough to produce RF burns on the skin underneath the coil. If surface coils are being used, they should be checked periodically using a phantom for proper detuning. If the detuning mechanism is losing effectiveness, artifacts will be seen in the test images owing to the retransmitted field producing its own excitation in the phantom near the coil. If a patient or subject reports a warm sensation under a surface coil during scanning, the scan should be stopped immediately. A similar concern exists for monitoring leads. The leads

used for electrocardiogram monitoring and other purposes can act as antennas to retransmit the RF field if they are allowed to form loops within the volume of the transmit coil. This can result in RF burns. It is very important that all monitoring leads be as straight as possible, and out of contact with bare skin as practical.

References

1. Bloch F. Nuclear induction. *Phys Rev.* 1946;70:460-474.
2. Bloch F et al. The nuclear induction experiment. *Phys Rev.* 1946;70:474-485.
3. Purcell EM, Torrey HC, Pound RV. Resonance absorption by nuclear magnetic moments in a solid. *Phys Rev.* 1946;69:37-38.
4. Hahn EL. Spin echoes. *Phys Rev.* 1950;80:580-594.
5. Lauterbur PC. Image formation by induced local interactions: examples employing nuclear magnetic resonance. *Nature.* 1973;242:190-191.
6. Lauterbur PC. Magnetic resonance zeugmatography. *Pure Appl Chem.* 1974;40:149-157.
7. Garroway AN, Grannell PK, Mansfield P. Image formation in NMR by a selective irradiative process. *J Phys C.* 1974;7:L457-L462.
8. Mansfield P, Maudsley AA. Medical imaging by NMR. *Br J Radiol.* 1977;50:188-194.
9. Twieg DB. The k-trajectory formulation of the NMR imaging process with applications in analysis and synthesis of imaging methods. *Med Phys.* 1983;10:610-621.
10. Zhu DC, Penn RD. Full-brain T_1 mapping through inversion recovery fast spin echo imaging with time-efficient slice ordering. *Magn Reson Med.* 2005;54:725-731.
11. Zaharchuk G, Martin AJ, Rosenthal G, Manley GT, Dillon WP. Measurement of cerebrospinal fluid oxygen partial pressure in humans using MRI. *Magn Reson Med.* 2005;54:113-121.
12. Wright PJ, Mougou OE, Totman JJ, et al. Water proton T_1 measurements in brain tissue at 7, 3, and 1.5 T using IR-EPI, IR-TSE, and MPRAGE: results and optimization. *Magn Reson Mater Phys.* 2008;21:121-130.
13. Schmitt P, Griswold MA, Jakob PM, et al. Inversion recovery true FISP: quantification of T_1 , Y_2 , and spin density. *Magn Reson Med.* 2004;51:661-667.
14. Lin C, Bernstein M, Huston J, Fain S. Measurements of T_1 relaxation times at 3.0 T: implications for clinical MRA. *Proc Intl Soc. Magn Reson Med.* 2001;9:1391.
15. Stanisz GJ, Odobina EE, Pun J et al. T_1 , T_2 Relaxation and magnetization transfer in tissue at 3 T. *Magn Reson Med.* 2005;54:507-512.
16. Deoni SCL. Transverse relaxation time (T_2) mapping in the brain with off-resonance correction using phase-cycled steady-state free precession imaging. *Magn Reson Imag.* 2009;30:411-417.
17. Deoni SCL, Ward HA, Peters TM, Rutt BK. Rapid T_2 estimation with phase-cycled variable nutation steady-state free precession. *Magn Reson Med.* 2004;52:435-439.
18. Madler B, Harris T, MacKay AL. 3D-Relaxometry – quantitative T_1 and T_2 brain mapping at 3 T. *Proc Intl Soc Magn Reson Med.* 2006;14:958.
19. Moran PR. A flow velocity zeugmatographic interlace for NMR imaging in humans. *Magn Reson Imag.* 1982;1:197-203.
20. Underwood SR, Firmin DN, Klipstein RH, Rees RS, Longmore DB. Magnetic resonance velocity mapping: clinical application of a new technique. *Br Heart J.* 1987;57:404-412.
21. Ahn CB, Kim JH, Cho ZH. High-speed spiral-scan echo planar NMR imaging. *IEEE Trans Med Imag.* 1986;5:2-7.
22. Meyer CH, Hu BS, Nishimura DG, Macovski A. Fast spiral coronary artery imaging. *Magn Reson Med.* 1992;28:202-213.
23. Mugler JP, Brookeman JR. Three-dimensional magnetization-prepared rapid gradient-echo imaging (3D MP RAGE). *Magn Reson Med.* 1990;15:152-157.
24. Sodickson DK, Manning WJ. Simultaneous acquisition of spatial harmonics (SMASH): fast imaging with radiofrequency coil arrays. *Magn Reson Med.* 1997;38:591-603.
25. Pruessmann KP, Weiger M, Scheidegger MB, Boesiger P. SENSE: sensitivity encoding for fast MRI. *Magn Reson Med.* 1999;42:952-962.
26. Madore B, Glover GH, Pelc NJ. Unaliasing by Fourier-encoding the overlaps using the temporal dimension (UNFOLD), applied to cardiac imaging and fMRI. *Magn Reson Med.* 1999;42:813-828.
27. Griswold MA, Jakob PM, Heidemann RM, et al. Generalized autocalibrating partially parallel acquisitions (GRAPPA). *Magn Reson Med.* 2002;47:1202-1210.

Brain Imaging in Behavioral Medicine and Clinical
Neuroscience

Cohen, R.A.; Sweet, L.H. (Eds.)

2011, XVI, 404 p. 10 illus. in color., Hardcover

ISBN: 978-1-4419-6371-0